Global and Planetary Change 200 (2021) 103461

Contents lists available at ScienceDirect

Global and Planetary Change

journal homepage: www.elsevier.com/locate/gloplacha

Determining the style and provenance of magmatic activity during the Early Aptian Oceanic Anoxic Event (OAE 1a)

L.M.E. Percival [a,*], L.R. Tedeschi [b], R.A. Creaser [c], C. Bottini [d], E. Erba [d], F. Giraud [e], H. Svensen [f], J. Savian [g], R. Trindade [h], R. Coccioni [i], F. Frontalini [j], L. Jovane [k], T.A. Mather [l], H.C. Jenkyns [l]

[a] Analytical, Environmental and Geochemistry (AMGC) Group, Vrije Universiteit Brussel, Pleinlaan 2, 1050 Brussels, Belgium
[b] Centro de Pesquisas e Desenvolvimento Leopoldo Américo Miguez de Mello (CENPES), Petróleo Brasileiro S.A., Avenida Horácio Macedo 950, 21941-915 Rio de Janeiro, Brazil
[c] Department of Earth and Atmospheric Sciences, University of Alberta, Edmonton, Alberta T6G 2E3, Canada
[d] Dipartimento di Scienze della Terra, Università degli Studi di Milano, 20133 Milan, Italy
[e] Université Grenoble Alpes, IRD, Université Savoie Mont Blanc, CNRS, Université Gustave Eiffel, ISTerre, 38000 Grenoble, France
[f] The Center for Earth Evolution and Dynamics, University of Oslo, PO Box 1028, Blindern, 0315, Oslo, Norway
[g] Departamento de Geologica, Universidade Federal do Rio Grande do Sul, 91501-970 Porto Alegre, Brazil
[h] Departamento de Geofísica, Universidade de São Paulo, 05508-090 São Paulo, Brazil
[i] Università degli Studi di Urbino "Carlo Bo", 61029 Urbino, Italy
[j] Dipartimento di Scienze Pure e Applicate, Università degli Studi di Urbino "Carlo Bo", 61029 Urbino, Italy
[k] Instituto Oceanográfico, Universidade de São Paulo, 05508-120 São Paulo, Brazil
[l] Department of Earth Sciences, University of Oxford, South Parks Road, Oxford, OX1 3AN, UK

ARTICLE INFO

Keywords:
Early Aptian Oceanic Anoxic Event (OAE 1a)
Mercury
Osmium isotopes
Greater Ontong-Java Plateau
High Arctic Large Igneous Province
Submarine LIP volcanism

ABSTRACT

Large igneous province (LIP) volcanism has been proposed as a key trigger of several major climate and environmental perturbations during the Phanerozoic Aeon. Large-scale carbon emissions associated with one or both of magmatic degassing from the Greater Ontong-Java Plateau (G-OJP) and intrusion of organic-rich sediments by High Arctic LIP (HALIP) sills have been widely suggested as the trigger of the Early Aptian Oceanic Anoxic Event (OAE 1a: ~120 Ma). However, the respective roles of the two LIPs and associated carbon sources in causing this crisis remain debated. Here, six records of OAE 1a from the Pacific, Tethyan, Arctic, and South Atlantic realms are investigated, combining mercury (Hg) concentrations and osmium- (Os-) isotope ratios as proxies of LIP activity. Together with previously published datasets, the results indicate globally consistent Os-isotope evidence for LIP activity during OAE 1a, but geographically variable stratigraphic Hg trends. Clear mercury enrichments that match Os-isotope evidence of LIP activity, and suggest a Hg-cycle perturbation during the onset of OAE 1a, are documented at one Pacific site extremely proximal to the G-OJP, but not in Arctic, Tethyan or Atlantic records. This pattern highlights significant G-OJP volcanism during the onset of OAE 1a, and re-emphasises the limited potential for submarine LIP eruptions to cause Hg-cycle perturbations except in areas very proximal to source. The absence of clear Hg peaks in basal OAE 1a strata from the Arctic (or anywhere outside of the Pacific) does not support intense HALIP activity at that time, suggesting that the G-OJP was the more volcanically active LIP when OAE 1a commenced. Thus, G-OJP emissions of mantle carbon were more likely to have played a major role in initiating OAE 1a than thermogenic volatiles associated with the HALIP. A transient pulse of HALIP-related subaerial eruptions and/or thermogenic volatile emissions during the early–middle part of OAE 1a, potentially evidenced by more widespread Hg enrichments in strata from that time (including in the Arctic), might have prolonged the event. However, a non-volcanic cause of these later Hg influxes cannot be excluded. These findings challenge previous suggestions that magmatic CO_2 emissions from LIPs were incapable of causing major carbon-cycle perturbations alone, and highlight the need for further investigations to establish whether the high volume/emplacement rate of the G-OJP (potentially an order of magnitude greater than other LIPs) made it a unique case that stands in contrast to other provinces where the role of thermogenic volatiles was likely more crucial.

* Corresponding author.
E-mail address: lawrence.percival@vub.be (L.M.E. Percival).

https://doi.org/10.1016/j.gloplacha.2021.103461
Received 12 October 2020; Received in revised form 25 January 2021; Accepted 1 March 2021
Available online 9 March 2021

1. Introduction

Episodes of abrupt environmental perturbation occurred frequently throughout the Mesozoic Era, punctuating and/or superimposed upon longer term changes in climate (e.g., Jenkyns, 2010). The Early Aptian Oceanic Anoxic Event (OAE 1a, ~120 Ma) represented one of the most severe of these crises. Lasting ~1–1.4 Myr (Li et al., 2008; Malinverno et al., 2010), the event was characterised by the development of oxygen-depleted water columns across large parts of the global ocean and epicontinental shelf seas (e.g., Schlanger and Jenkyns, 1976; Weissert, 1989; Jenkyns, 1995; Pancost et al., 2004; Föllmi et al., 2006; van Breugel et al., 2007). Ocean acidification, global temperature changes, accelerated hydrological cycling, and enhanced continental weathering rates have also been proposed to have occurred at that time (e.g., Erba, 2004; Ando et al., 2008; Erba et al., 2010, 2015; Bottini et al., 2012, 2015; Hönisch et al., 2012; Mutterlose et al., 2014; Lechler et al., 2015; Naafs and Pancost, 2016; Jenkyns, 2018). The various environmental perturbations are thought to have arisen from (and in some cases, contributed to) severe carbon-cycle disturbances. These perturbations are reflected by a series of carbon-isotope ($\delta^{13}C$) excursions documented from lower Aptian strata that record OAE 1a; typically interpreted via comparison to segments (C1–C7) in the stratigraphic $\delta^{13}C$ trends first recorded in Tethyan pelagic sedimentary archives (Menegatti et al., 1998; see also Fig. 1A, and Weissert, 1989; Jenkyns, 1995; Gröcke et al., 1999; Ando et al., 2008; Robinson et al., 2008; Vickers et al., 2016). Relatively stable $\delta^{13}C$ values spanning uppermost Barremian–lowermost Aptian strata (C1–C2) give way to a pronounced negative excursion in basal OAE 1a strata (C3), which is followed by two distinct positive excursions (C4 and C6) that are locally separated by strata featuring stable carbon-isotope ratios higher than those of C2 (C5), and are succeeded by a continuation of high $\delta^{13}C$ values (C7) above the OAE 1a stratigraphic level (Menegatti et al., 1998; see also Fig. 1A).

The two positive $\delta^{13}C$ excursions that typically signify the C4 and C6 segments are thought to record enhanced rates of organic-matter burial in the widespread anoxic–euxinic water columns that characterised OAE 1a (e.g., Weissert, 1989; Menegatti et al., 1998). Such organic-matter deposition is further evidenced by the preservation of organic-rich shales in several stratigraphic archives of the event worldwide (e.g., Schlanger and Jenkyns, 1976; Erba and Larson, 1998; Dumitrescu and Brassell, 2006; Hu et al., 2012; Robinson et al., 2017). Initially recognised in the Umbria–Marche Basin of Italy (Coccioni et al., 1987), the organic-rich shale unit is named the Selli Level in that region, with sedimentary rocks of OAE 1a age (whether comprising organic-rich shales or otherwise) elsewhere around the world dubbed the Selli Level Equivalent (see Fig. 1 and Study Areas section).

By contrast, the C3 negative $\delta^{13}C$ shift is attributed to a pronounced flux of isotopically light carbon to the ocean–atmosphere system that likely initiated the environmental perturbations associated with OAE 1a (e.g., Jahren et al., 2001; Méhay et al., 2009; Kuhnt et al., 2011; Naafs et al., 2016). The source of this isotopically light carbon remains debated. Several authors have linked the carbon emissions to the emplacement of one or more large igneous provinces (LIPs) during earliest Aptian times, particularly the Greater Ontong-Java Plateau (G-OJP; Fig. 2; see e.g., Erba, 1994; Larson and Erba, 1999; Tejada et al., 2009; Kuroda et al., 2011; Bottini et al., 2012; Erba et al., 2015; Polteau et al., 2016).

Geochemical modelling by Bauer et al. (2017) indicated that the emplacement of the G-OJP resulted in a geologically rapid six- to ten-fold increase in submarine volcanic activity during OAE 1a, and that such volcanism could have caused a fourfold rise in mantle carbon emissions ($\delta^{13}C \sim -6‰$; Gales et al., 2020, and references therein). These emissions alone could have plausibly caused a similarly swift 3000 ppm increase in atmospheric pCO_2 levels and the 1.5–2‰ negative $\delta^{13}C$ excursion typically documented in the C3 segment. However, based on pCO_2 trends reconstructed from the Cau section (Betic Cordillera, Spain), Naafs et al. (2016) argued that pCO_2 levels only rose gradually through the first part of OAE 1a and by <300 ppm during the C3 segment. In this case, a much smaller increase in carbon emissions, but with a very isotopically light composition ($\delta^{13}C < -10‰$), would have been required to cause the C3 negative excursion without greatly increasing atmospheric pCO_2 (Adloff et al., 2020). Such parameters are inconsistent with a purely mantle-carbon source. Instead, this carbon could have been emitted following metamorphism of organic-rich sediments by intrusive sills during the emplacement of the High Arctic large igneous province (HALIP; Fig. 2), or from the destabilisation of methane clathrates (e.g., Jahren et al., 2001; Méhay et al., 2009; Polteau et al., 2016; Adloff et al., 2020). This study investigates the geochemical records of volcanism related to the emplacement of the G-OJP and HALIP during the earliest Aptian and OAE 1a in order to determine the dominant style of magmatic activity operating during those times. This distinction might indicate whether or not a specific igneous province was the foremost source of carbon to the ocean–atmosphere system and likely the key trigger of the event.

1.1. Large igneous provinces emplaced during the latest Barremian and early Aptian

The G-OJP was an oceanic LIP consisting of several million cubic kilometres of igneous material (largely tholeiitic basalt) emplaced as intrusive and extrusive magma bodies into/onto the ocean crust of the western Pacific (Fig. 2; see also Larson, 1991; Larson and Erba, 1999).

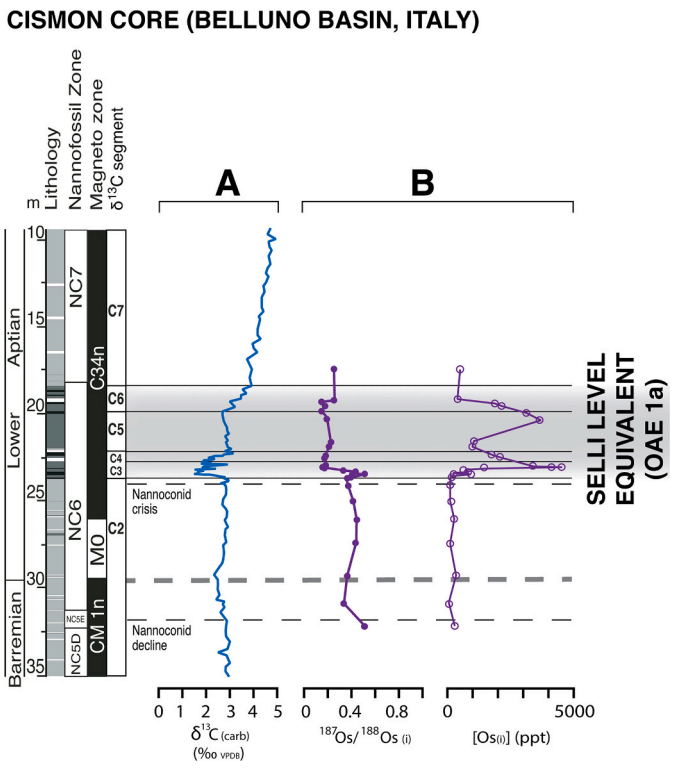

Fig. 1. Previously published trends across the Selli Level Equivalent of the Cismon core for A) carbon isotopes and B) osmium isotopes and osmium concentrations (data from Erba et al., 1999; Bottini et al., 2012). The grey shaded area indicates the stratigraphic extent of Selli Level Equivalent sediments deposited during OAE 1a; the dashed grey line the Barremian–Aptian boundary at the base of magnetozone M0 (Erba et al., 1999; Channell et al., 2000; Bottini et al., 2012). The stratigraphic levels of both the decline and crisis of nannoconids (Erba et al., 1999) are indicated by thin dashed black lines, and the $\delta^{13}C$ segments (from Menegatti et al., 1998) by solid thin black lines. See methods section for details on the calculation of initial seawater Os-isotope ratios ($^{187}Os/^{188}Os_{(i)}$) and sedimentary osmium concentrations ($[Os_{(i)}]$). Lithology, biostratigraphy, magnetostratigraphy, and carbon-isotope segments are sourced as for Fig. 4.

The Ontong-Java Plateau alone has an immense volume of 10s of millions of cubic kilometres (possibly up to 44–57 × 10^6 km^3; Gladczenko et al., 1997). When other subsidiary plateaus thought to have initially formed as part of the G-OJP are included (e.g., the Manihiki and Hikurangi; Taylor, 2006; Hoernle et al., 2010), the total volume of igneous material rises to 59–77 × 10^6 km^3 (Kerr and Mahoney, 2007). The original province may have been even larger if a part of it was emplaced into/onto the now-subducted Farallon Plate, as has been previously suggested (Schlanger et al., 1981; Larson, 1991). Thus, the G-OJP could have been an order of magnitude greater in size than the largest-known continental LIPs: the Siberian Traps and Central Atlantic Magmatic Province, which were likely no more than ~5 × 10^6 km^3 each in volume (see review by Bond and Wignall, 2014). The average eruption rate on the G-OJP remains unknown. However, if Bauer et al.'s (2017) calculation of a six- to ten-fold increase in submarine volcanic activity during OAE 1a compared to pre-OAE background mid-ocean ridge volcanism is correct, and ridge basalt production during Barremian–Aptian times was similar to today (~20 km^3/yr; Cogné and Humler, 2006), then on average > 100 km^3/yr of igneous material would have been emplaced on the G-OJP during OAE 1a. This average eruption rate is markedly higher than that proposed for any known continental LIP (e.g., Schoene et al., 2019).

By contrast, Barremian–Aptian HALIP magmatism apparently consisted chiefly of subaerially erupted basalt flows and the intrusion of tholeiitic sills into organic-rich sedimentary rocks (Tegner et al., 2011; Corfu et al., 2013; Polteau et al., 2016; Dockman et al., 2018). The volume of HALIP igneous material emplaced during Barremian–Aptian times remains poorly constrained, but is thought to have been on the order of 100,000 s of cubic kilometres (Tegner et al., 2011; Polteau et al., 2016; Dockman et al., 2018), much smaller than the G-OJP but more comparable in volume to many other LIPs. However, the intrusion of organic-rich sediments by HALIP magmatic sills could have acted as an additional source of isotopically light carbon ($\delta^{13}C < -20‰$) to the ocean–atmosphere system (Polteau et al., 2016; c.f., Svensen et al., 2004; McElwain et al., 2005). By contrast, carbon emissions from the G-OJP would have been almost exclusively magmatic in origin, as that LIP was predominantly emplaced into comparatively volatile-depleted oceanic basalts.

Crucially, although there is some evidence from phreatomagmatic deposits dated to ~120 Ma for subaerial eruptions on the G-OJP during Barremian–Aptian times (Chambers et al., 2004; Thordarson, 2004), the emplacement of that province into/onto the oceanic crust means that the great majority of volcanic activity associated with it is expected to have been submarine in nature. By contrast, most volatile emissions from HALIP subaerial basalts and thermogenic degassing should have reached the atmosphere. Previous studies have highlighted the fact that geochemical markers of LIP volcanism in stratigraphic archives may be able to distinguish between these styles of magmatic processes, and also yield information on the proximity of the igneous activity (Kuroda et al., 2011; Erba et al., 2015). In particular, Percival et al. (2018) noted the differing degrees to which styles of volcanism can affect the likelihood of LIP emplacement and associated eruptions being recorded by two key proxies for these phenomena: mercury (Hg) concentrations and osmium- (Os-) isotope ratios (specifically $^{187}Os/^{188}Os$).

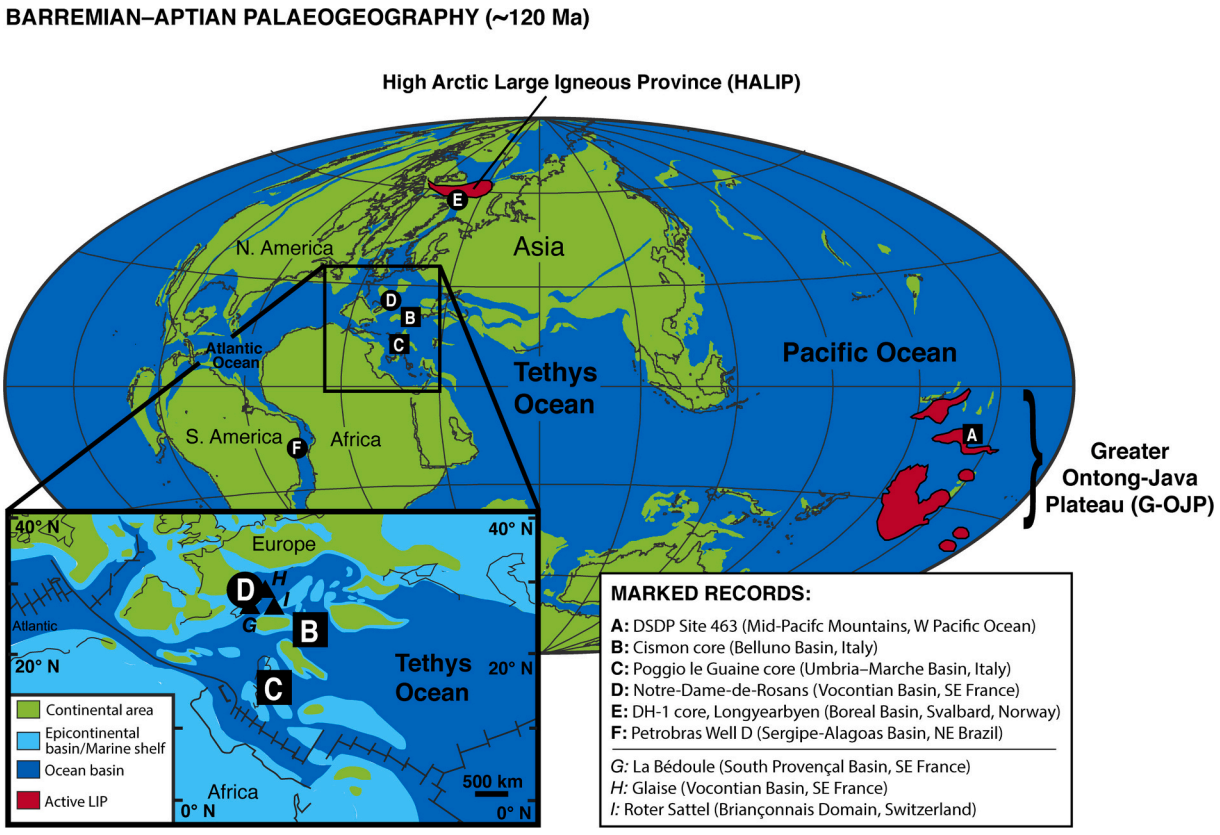

Fig. 2. Palaeogeographic map of the Barremian–Aptian world (~120 Ma). The positions of the HALIP and G-OJP are indicated by dark red areas. Locations A–F mark sites of sedimentary records investigated for mercury in this study (black squares = mercury and osmium-isotope data presented; black circles = mercury data presented). Locations G–I (black triangles) indicate sites previously studied for mercury by Charbonnier and Föllmi (2017). Global map is adapted from van Breugel et al. (2007), with the western Tethys inset adapted from Giraud et al. (2018). (For interpretation of the references to colour in this figure legend, the reader is referred to the web version of this article.)

1.2. Sedimentary $^{187}Os/^{188}Os$ ratios as a marker of LIP emplacement during OAE 1a

Large igneous province emplacement can cause a change in the $^{187}Os/^{188}Os$ composition of the global ocean by acting as a major source of mantle-derived osmium, through either direct emission of the element during submarine volcanic/hydrothermal activity, or weathering/alteration of juvenile LIP basalts (e.g., Cohen and Coe, 2002; Turgeon and Creaser, 2008). Importantly, the seawater residence time of osmium (on the order of 10s kyr today: Peucker-Ehrenbrink and Ravizza, 2000) means that the global ocean should feature a homogenous $^{187}Os/^{188}Os$ composition but still respond to geologically rapid changes in the sources to that inventory, except in hydrographically restricted basins with a very low basin–ocean water-mass exchange where the Os-isotope ratio might be dominated by local inputs (e.g., Paquay and Ravizza, 2012; Dickson et al., 2015).

Primitive osmium derived from mantle or meteoritic material features $^{187}Os/^{188}Os \sim 0.13$ (Allègre et al., 1999), whereas riverine osmium sourced from weathering of the continental crust is typically much more radiogenic (modern-day average riverine $^{187}Os/^{188}Os \sim 1.4$; Peucker-Ehrenbrink and Jahn, 2001). Consequently, a significant increase in the flux of mantle-derived Os from LIP activity to the global ocean, relative to riverine runoff of the element from weathering of the continental crust and the comparatively consistent mid-ocean-ridge and cosmogenic inputs, should result in a lower seawater $^{187}Os/^{188}Os$ ratio throughout the open ocean. This hydrogenous Os-isotope signature is recorded in seafloor sediments, which can preserve past seawater compositions as long as the sedimentary system remains closed with respect to rhenium and osmium following deposition (Cohen et al., 1999).

In all previously studied records of OAE 1a, a pronounced shift is observed in the recorded seawater Os-isotope ratio ($^{187}Os/^{188}Os_{(i)}$) towards very unradiogenic compositions (typically <0.2) around the base of the Selli Level or equivalent strata , together with an increase in sedimentary Os concentrations (Tejada et al., 2009; Bottini et al., 2012; Adloff et al., 2020; see also Fig. 1B). These unradiogenic $^{187}Os/^{188}Os_{(i)}$ compositions and high Os concentrations generally continue up the stratigraphy through the entire Selli Level (or equivalent), and are thought to document intense LIP volcanism that acted as a source of osmium to the global ocean through one or both of submarine hydrothermal emissions of the element and erosion/alteration of the juvenile basalts formed during the volcanic activity (Tejada et al., 2009; Bottini et al., 2012; Adloff et al., 2020). However, Tethyan records of OAE 1a also document a brief rebound in Os-isotope ratios to higher values in basal Selli Level (or equivalent) strata, potentially highlighting a transient spell of enhanced continental weathering and associated flux of radiogenic Os at the onset of the event that temporarily overprinted the unradiogenic signature (Tejada et al., 2009; Bottini et al., 2012). This transient pulse of enhanced continental weathering early in OAE 1a is supported by strontium- and lithium-isotope excursions (Jones and Jenkyns, 2001; Lechler et al., 2015).

1.3. Sedimentary Hg concentrations as a marker of LIP volcanism during OAE 1a

Volcanic eruptions represent one of the largest natural sources of mercury to the Earth's surface in the present day (Pyle and Mather, 2003; Bagnato et al., 2007). Mercury is chiefly emitted as a gaseous elemental species that typically has a residence time of 0.5–2 years in the stratosphere, enabling worldwide distribution before the element is ultimately deposited in sediments (Schroeder and Munthe, 1998; Ericksen et al., 2003; Selin, 2009). The global distribution of volcanic mercury has led several studies of geological events associated with LIPs to utilise sedimentary concentrations of the element as a proxy for the postulated volcanism (see reviews by Grasby et al., 2019; Percival et al., 2021). This approach includes normalising sedimentary mercury concentrations against total organic carbon (TOC) content to account for the association of the element with organic compounds when it is deposited in sediments (Sanei et al., 2012, and references therein). Thus, peaks in sedimentary Hg/TOC ratios are generally interpreted as reflecting an increased input of Hg to the environment from an external source, such as volcanism or wildfires, the latter of which is also known to cause peaks in sedimentary Hg and Hg/TOC values in modern settings (e.g., Daga et al., 2016).

However, in euxinic settings where free sulphides precipitate in the water column, Hg may be deposited with that phase rather than organic matter (Shen et al., 2019a; Shen et al., 2020). Alternatively, in a very well-oxygenated environment, featuring limited burial of both phases, mercury might be adsorbed on to clays (Kongchum et al., 2011; Shen et al., 2020). Even in settings where Hg contents follow those of TOC, a change in the type of organic matter (e.g., from marine bacterial to terrestrial detrital), or a large influx of it from a new source, could alter the Hg/TOC ratio if the affinity of mercury for the various kinds of organic material varies (see Hammer et al., 2019; Them et al., 2019). Therefore, robustly demonstrating a global-scale perturbation to the mercury cycle caused by volcanism is dependent on documenting enrichment of the element in stratigraphic archives that cover a wide range of geographic areas, and for which the depositional environment and burial history are known.

To date, three stratigraphic archives of OAE 1a have been investigated for mercury and Hg/TOC trends by Charbonnier and Föllmi (2017), all of them representing palaeoenvironments from the northwesternmost part of the Tethyan realm: La Bédoule (South Provençal Basin, SE France), Glaise (Vocontian Basin, SE France), and Roter Sattel (Briançonnais Domain, Switzerland). This last record has been shown as being rather thermally mature (Charbonnier et al., 2018a), potentially altering the TOC content and inflating measured Hg/TOC ratios to above those from the time of deposition (as shown for other Cretaceous records by Charbonnier et al., 2020). Nonetheless, Charbonnier and Föllmi (2017) reported increased Hg and Hg/TOC values that were ascribed to G-OJP volcanic activity during OAE 1a (see also Supplementary Fig. 1). Interestingly, Barremian–Aptian boundary records from the northwest Tethyan area have also been hypothesised as recording an earlier episode of volcanism associated with that LIP, which took place significantly prior to OAE 1a (Charbonnier et al., 2018b).

1.4. Study aims

Whilst mercury-cycle perturbations from Barremian–Aptian times (including OAE 1a) have been reported from the northwest Tethyan area, and linked to volcanism on the G-OJP, it remains unclear whether these disturbances truly represent a global volcanic signal or local influxes of mercury to that specific region. In this context, it is notable that mercury emitted from modern submarine volcanic systems appears to be efficiently scavenged, limiting dispersal of the element from such sources to areas relatively proximal to the point(s) of origin (within 100s km; Bowman et al., 2015). Indeed, prior investigations of the latest Cenomanian OAE (OAE 2; ~94 Ma), which has also been linked with submarine LIP volcanism during oceanic-plateau emplacement (e.g., Turgeon and Creaser, 2008), have shown that most studied records of that event do not feature Hg enrichments or elevated Hg/TOC ratios, except perhaps for sites proximal to LIPs (Scaife et al., 2017; Percival et al., 2018).

Consequently, analyses of stratigraphic archives of OAE 1a from around the world are needed in order to determine whether there was global-scale Hg-cycle perturbation during that event, or localised disturbances unrelated to magmatism. Furthermore, a global perspective of the mercury cycle will help to elucidate whether any volcanic fluxes of mercury were largely derived from G-OJP or HALIP activity. If volatile emissions during OAE 1a were primarily associated with submarine LIP activity of the G-OJP, sedimentary mercury enrichments correlative with the Os-isotope evidence of volcanism would likely be recorded in

Pacific sites proximal to that source, but potentially nowhere else due to the limited dispersal range of the element in the marine realm. By contrast, mercury fluxes from subaerial eruptions and/or thermogenic emissions related to the HALIP should certainly be observed in Arctic records, and might also be documented in sites around the world due to those magmatic processes being more likely to emit volatiles directly to the atmosphere.

Here, new mercury data are presented from six records of latest-Barremian–early Aptian age, including OAE 1a (Fig. 2): DSDP Site 463 (Mid-Pacific Mountains), the Cismon core (Belluno Basin, Italy), the Poggio le Guaine core (Umbria–Marche Basin, Italy), the Notre-Dame-de-Rosans section (Vocontian Basin, SE France), the DH-1 Longyearbyen core (Boreal Basin, Svalbard), and the Petrobras Well D (Sergipe-Alagoas Basin, NE Brazil). New Os-isotope data are also presented from the Poggio le Guaine core. These sequences include the first OAE 1a records from outside the Tethyan region that have been studied for mercury, offering a more global perspective on any Hg-cycle perturbations during that time. Crucially, these study areas include three sites where stratigraphic Hg and Os-isotope trends can be directly correlated (DSDP Site 463 and the Cismon and Poggio le Guaine cores). Additionally, the Mid-Pacific Mountain and Arctic sites would have been relatively proximal to the G-OJP and HALIP, respectively. Comparing these new mercury and osmium-isotope profiles with previously published datasets, and correlating trends in the two proxies amongst records where both have been studied, will give new insights on the dominant style of volcanic activity that influenced the global Hg cycle during OAE 1a and could potentially identify the LIP that was the primary trigger of that event.

2. Study areas

2.1. DSDP Site 463 (Mid-Pacific Mountains, W Pacific Ocean)

DSDP Site 463, drilled in the Mid-Pacific Mountains in 1978, records a large part of the uppermost Barremian to lower Aptian stratigraphic interval (Thiede et al., 1981). The lithology generally consists of pelagic limestones with some chert-rich intervals (Mélières et al., 1981). There is a switch to more clay-rich marlstones between ~625–615 mbsf that marks the OAE 1a stratigraphic interval (Thiede et al., 1981; Sliter, 1989). However, black shales akin to those observed in most Tethyan archives are largely absent from this site and only appear in upper Selli Level Equivalent strata, with a modest increase in TOC content (to 1.5 wt %, *this study*; although previous works have reported values locally up to 7–8 wt%; Thiede et al., 1981; van Breugel et al., 2007; Bottini et al., 2012). Age constraints (including the position of the Barremian–Aptian boundary) are based largely on magneto- and biostratigraphy (Tarduno et al., 1989). Several studies have investigated the Barremian–Aptian carbon-isotope trends at DSDP Site 463 (e.g., Price, 2003; Ando et al., 2008; Bottini et al., 2012), identifying the C2–C7 segments that can be used to define the Selli Level Equivalent strata deposited during OAE 1a. Osmium-isotope trends and trace-metal enrichments have been interpreted as evidence for intense volcanic activity during Barremian–Aptian times (particularly before and during OAE 1a), with the volcanism generally attributed to the nearby G-OJP (Bottini et al., 2012; Erba et al., 2015). Volcanic eruptions proximal to DSDP Site 463 are supported by sporadic preservation of thin tuffaceous layers locally preserved within the Barremian–Aptian sediments; particularly within the Selli Level Equivalent (Hein and Vanek, 1981; Vallier and Jefferson, 1981; Thiede et al., 1982). The provenance of these tuffs remains unknown, but given the proximity of the Mid-Pacific Mountains to the G-OJP, eruptions on that volcanically active LIP would be a plausible source.

2.2. Cismon core (Belluno Basin, Italy)

The Cismon core was drilled in the Southern Alps north-west of Treviso (Italy) in 1995, and is one of the best-studied latest Barremian–Aptian Tethyan records (Erba and Larson, 1998). The core largely consists of pale-coloured pelagic carbonates deposited on the slope of the Belluno Basin. However, the Selli Level Equivalent is marked by a clear lithological change to organic-rich marlstones and shales interbedded with sporadic radiolarian-rich beds (Erba and Larson, 1998). The increase in TOC, together with elevated sulphur contents and preservation of the biomarker isorenieratane in some Selli Level Equivalent beds, strongly supports the development of at least periodically euxinic conditions in the Belluno Basin during OAE 1a (van Breugel et al., 2007; Bottini et al., 2012). Magneto-, bio-, and carbon-isotope stratigraphy provide excellent temporal constraints, with all the $\delta^{13}C$ excursions and C1–C8 segments well preserved (Menegatti et al., 1998; Erba et al., 1999; Channell et al., 2000). A pronounced decline in the abundance of nannoconids has been documented just below the Barremian–Aptian boundary, with a further reduction (to almost nothing) of these nannofossils near the base of the Selli Level Equivalent (Erba, 1994). These changes in the fossil record highlight the biotic impact of the environmental perturbations that took place prior to and during OAE 1a (e.g., Bralower et al., 1994; Erba, 1994; Erba and Tremolada, 2004; Erba et al., 2010). Age modelling of lower Aptian strata from the Cismon core have indicated dates for the Barremian–Aptian transition and OAE 1a that overlap with G-OJP basalt ages (see Malinverno et al., 2010; Erba et al., 2015). Furthermore, both osmium-isotope trends (see above) and enrichments in several trace metals of probable mafic derivation in Barremian–Aptian strata provide direct evidence of LIP activity at that time (Bottini et al., 2012; Erba et al., 2015).

2.3. Poggio le Guaine core (Umbria–Marche Basin, Italy)

The Poggio le Guaine (PLG) core was drilled in 2010 in the Northern Apennines at a site 6 km to the west of the city of Cagli (Coccioni et al., 2012), close to a previously studied lower Aptian outcrop that includes sediments of OAE 1a age deposited as the Selli Level *sensu stricto* (e.g., Lowrie et al., 1980; Coccioni et al., 1987, 1990; Baudin et al., 1998). Like the outcrop section, the core represents a well-preserved and apparently continuous Aptian–Albian succession that records a pelagic environment in the Umbria–Marche Basin of the north-western Tethyan area. The lithology is dominated by white and grey nannofossil-foraminiferal pelagic limestones, with rare cherts, radiolarian-rich beds, and green limestones (Coccioni et al., 2012; Savian et al., 2016). Stratigraphic age constraints on the position of the Barremian–Aptian boundary are based on magnetostratigraphy and calcareous planktonic foraminiferal biostratigraphy (Coccioni et al., 2012; Savian et al., 2016). Intercalated organic-rich shales and radiolarian-rich beds, an overall relative elevation in TOC contents, and a negative (C3) and recovery/broad positive excursion (C4–C6) in carbonate $\delta^{13}C$ ratios all define the Selli Level (89.24–91.29 m; Coccioni et al., 2012; Savian et al., 2016; *this study*). However, within the OAE 1a strata there is a black-shale unit containing insufficient carbonate for carbon-isotope analysis, leaving a gap in the $\delta^{13}C$ trends that hinders precise placement of the C4–C5 and C5–C6 boundaries (~89–91 m).

2.4. Notre-Dame-de-Rosans (Vocontian Basin, SE France)

The Vocontian Basin was one of a number of large epicontinental depocentres located in the north-western area of the Cretaceous Tethys Ocean, formed by tectonic processes related to the opening of the Bay of Biscay (e.g., Hibsch et al., 1992), with basinal clay-rich calcareous hemipelagic sediments preserved today in south-eastern France (Bréhéret, 1997). The Notre-Dame-de-Rosans section provides an excellent record of OAE 1a in the Vocontian Basin, comprising interbedded clay-rich calcareous marls and fine-grained turbidites (Giraud et al., 2018). The stratigraphy can be correlated with other archives from that region, and elsewhere, based on biostratigraphic constraints, its carbon-isotope record (clearly documenting the C2–C7 segments),

and the preservation of less calcareous, darker coloured, TOC-enriched grey marls in the upper part of the Selli Level Equivalent (Giraud et al., 2018), locally named the Niveau Goguel (Bréhéret, 1998). This organic matter is immature and appears to be largely composed of marine algal/bacterial material, but potentially with some contribution from degraded/terrestrially derived debris (Giraud et al., 2018). Based on the identification of <6 μm framboidal pyrite and cyanobacterial biomarkers in the Niveau Goguel strata of the nearby Les Sauzeries section (<50 km away), it has been inferred that anoxic–euxinic settings developed during the latter part of OAE 1a (Ando et al., 2013; Giraud et al., 2018). However, such conditions were likely intermittent, with the turbidite flows reventilating the marine environment (Caillaud et al., 2020).

2.5. DH-1 core, Longyearbyen (Boreal Basin, Svalbard, Norway)

The western part of Svalbard records a very near-shore shallow-marine palaeoenvironment in an epicontinental basin, with a lithology consisting of mudstone–siltstone beds, fluvial–marginal marine sandstone lenses, and coals (Midtkandal et al., 2016; Vickers et al., 2016). Macroscopic higher-plant debris in DH-1 core samples supports a dominantly terrestrial source of organic matter, further evidenced by low measured hydrogen index (HI) values, although the low HI could partly/completely result from the high thermal maturity of the sediments (Midtkandal et al., 2016). A limited quantity of marine palynomorphs allows for dinoflagellate biostratigraphy, from which a broadly Barremian–Aptian age for the interval of the DH-1 core studied here has been determined (Midtkandal et al., 2016). A negative $\delta^{13}C$ excursion and positive shift immediately stratigraphically above it (150.47–133.37 m) are thought to be equivalent to the C3 and C4–C6 segments, respectively, and have been interpreted as marking the Selli Level Equivalent strata in the core (Midtkandal et al., 2016). Further subdivision of the C4–C6 segments is not possible due to the low resolution of the $\delta^{13}C$ dataset. Interestingly, TOC contents decrease to an average of 1.8 wt% within the Selli Level Equivalent, compared to mean quantities of 3.8 wt% and 3.3. wt% in sediments stratigraphically above and below, respectively (Midtkandal et al., 2016). For this study, mercury analyses were limited to mudstone layers, avoiding sandstone/coal beds, in order to maintain relative consistency in terms of the lithology and organic-matter content of the studied samples, as previous works have shown that major lithological variations can strongly influence Hg concentrations and Hg/TOC variations independently of any potential external source (e.g., Percival et al., 2018).

2.6. Petrobras Well D (Sergipe-Alagoas Basin, NE Brazil)

The Sergipe-Alagoas Basin was one of a number of rift-basins along the eastern and southern part of Brazil that formed during the Early Cretaceous as a result of the opening of the South Atlantic Ocean (Chaboureau et al., 2013, and references therein). The Petrobras Well D was drilled through the Muribeca and Riachuelo Formations of the basin, consisting of sandy and conglomeratic siliciclastics interbedded with siltstones and mudstones, the last of which are locally calcareous. Taken together, the stratigraphic sequence is interpreted as having been deposited in a continental–coastal setting that was initially dominated by fluvio-deltaic systems, but gradually transitioned towards lacustrine/lagoonal settings due to continuing basin subsidence as rifting of the South Atlantic proceeded (Tedeschi et al., 2020). Elsewhere in the Sergipe-Alagoas Basin, the Riachuelo Formation has been dated as late Aptian in age on the basis of planktonic foraminiferal biostratigraphy (e.g., Koutsoukos, 1992), with the underlying Muribeca Formation generally accepted as also having been deposited (earlier) in the Aptian (Tedeschi et al., 2020). Consequently, a series of pronounced carbon-isotope excursions near the bottom of the Muribeca Formation in the Petrobras Well D core has been interpreted as marking the Selli Level Equivalent, with a negative excursion overlain by two positive shifts interpreted as the C3 and C4–C6 segments, respectively (Tedeschi et al., 2020). TOC contents are variable, ranging from <0.1 wt% up to 5.2 wt %, with mean values highest in the postulated C5 strata, and primarily composed of detrital terrestrial organic matter that has locally been oxidised, based on the determined hydrogen and oxygen indices and the nature of the recorded palaeoenvironment (Tedeschi et al., 2020).

3. Methods

Mercury data for all records were generated using a RA-915 Portable Mercury Analyzer with PYRO-915 Pyrolyzer, Lumex, at the University of Oxford (UK). Analyses were carried out following the methodology in Percival et al. (2017), with at least two analyses conducted for each sample. Two reference materials were utilised as standards for machine calibration and drift check throughout a set of analyses: NIMT/UOE/FM/001 – Inorganic Elements in Peat (169 ppb Hg) and NIST-SRM2587 – Trace Elements in Soil Containing Lead from Paint (290 ppb Hg). Analytical uncertainty based on repeated measurements of the reference materials was ±15 ppb. Concentrations of other metals in the DH-1 core samples were measured by ICP-AES at Imperial College London (UK) following preparation by lithium metaborate fusion and hydrofluoric/perchloric acid digestion, after the methods in Neumann et al. (2013).

New TOC data were generated by Rock-Eval 6 analysis for samples from DSDP Site 463, the Cismon core, and Notre-Dame-de-Rosans, at the University of Oxford, after the methodology of Behar et al. (2001). Repeated measurements of an internal mudrock standard SAB134 (calibrated to the International reference material IFP 160000) were used to assess analytical accuracy and repeatability, and yielded an average value of 2.81 ± 0.07 wt%, consistent with long-term measurements for the laboratory (2.87 ± 0.11 wt%; Storm et al., 2020), and indicating analytical uncertainty better than 0.1 wt% (1σ). New TOC data for PLG core samples were determined on a Strohlein Coulomat 702 at the University of Oxford, using the procedure in Jenkyns (1988). TOC contents have been previously determined using Rock Eval and Leco SC-632 instruments for all samples from the DH-1 core and Petrobras Well D analyzed for mercury in this study, at the Institute for Energy Technology, Kjeller (Norway) for the DH-1 core (Midtkandal et al., 2016), and at the Universities of Oxford and Universidade do Estado do Rio de Janeiro for Petrobras Well D (Tedeschi et al., 2020). The new data from the Cismon core were combined with published values that were generated at the Open University (UK) using a Leco CNS-2000 elemental analyser (Bottini et al., 2012).

New osmium-isotope data were determined for ten samples from the PLG core following the methodology outlined in Kendall et al. (2015), with eight samples taken from the Selli Level, and two others from beneath the base of it. Sample preparation utilised Carius-tube digestion with $Cr^{VI}O_3$-H_2SO_4, with subsequent Os purification using established solvent extraction (by chloroform) and microdistillation techniques (Selby and Creaser, 2003). Rhenium purification was carried out with solvent extraction using sodium hydroxide and acetone, and subsequent anion exchange chromatography (Cumming et al., 2013). Isotopic compositions and concentrations of rhenium and osmium were determined by isotope dilution and negative thermal ionisation mass spectrometry (N-TIMS) on a Thermo Triton instrument at the Department of Earth and Atmospheric Sciences, University of Alberta (Canada). Total procedural blanks for osmium and rhenium were 0.3 and 15 pg, respectively, whilst the $^{187}Os/^{188}Os$ composition of the blanks was 0.20. In-house standard solutions for osmium (AB2; see e.g., Selby, 2007; Finlay et al., 2010) and rhenium (ICP-MS standard rhenium solution of normal isotopic composition) yielded values in agreement with previous studies (van Acken et al., 2013; Kendall et al., 2015): $^{187}Os/^{188}Os$ of 0.10684 ± 0.00015 (1σ) for osmium, and $^{185}Re/^{187}Re$ of 0.59778 ± 0.00077 (1σ) for rhenium.

The past seawater composition at the time of deposition ($^{187}Os/^{188}Os_{(i)}$) is determined from the modern-day $^{187}Os/^{188}Os$ ratio of a sedimentary rock sample using its age and its Re and Os concentrations

to account for the post-depositional decay of rhenium (^{187}Re) to ^{187}Os (Cohen et al., 1999). The osmium concentration of a sedimentary rock at the time of its deposition is determined from the modern-day osmium concentration after accounting for the post-depositional decay of ^{187}Re to ^{187}Os, by using the difference between the measured modern-day ^{187}Os/^{188}Os ratio and the calculated ^{187}Os/^{188}Os$_{(i)}$ value, together with the ^{192}Os content of the rock and the known natural ^{192}Os/^{188}Os isotope ratio (see Supplementary Text).

4. Results

4.1. Os-isotope and osmium concentration data from the PLG core

Following correction of the measured modern-day Os-isotope ratio for decay of rhenium since deposition at 120 Ma, the recorded ^{187}Os/^{188}Os$_{(i)}$ values show a clear shift from ~0.6 to ~0.2 in the basal Selli Level strata (Fig. 3). There is also a notable increase in the calculated [Os$_{(i)}$] concentrations across that horizon, from 149 ppt in the stratigraphically lowest analyzed sample to a maximum of 3719 ppt in the middle of the Selli Level. These trends are broadly consistent with osmium trends from Gorgo a Cerbara, Cismon (both Italy), DSDP Site 463 (Pacific), and Cau (Spain) reported by previous studies (Tejada et al., 2009; Bottini et al., 2012; Adloff et al., 2020). Interestingly, the transient shift to more radiogenic ^{187}Os/^{188}Os$_{(i)}$ values documented from other Tethyan records (Cismon and Gorgo a Cerbara; Tejada et al., 2009; Bottini et al., 2012; see Fig. 1) is not observed in the PLG data. This lack of ^{187}Os/^{188}Os$_{(i)}$ spike in the PLG core may result from the absence of data from below the Selli Level at that site (Fig. 3). Alternatively, the ^{187}Os/^{188}Os$_{(i)}$ spike may not be captured by the PLG dataset due to its relatively low-resolution, or the presence of a small hiatus/condensed layer at the base of the Selli Level, although there is no sedimentological evidence for such a stratigraphic gap.

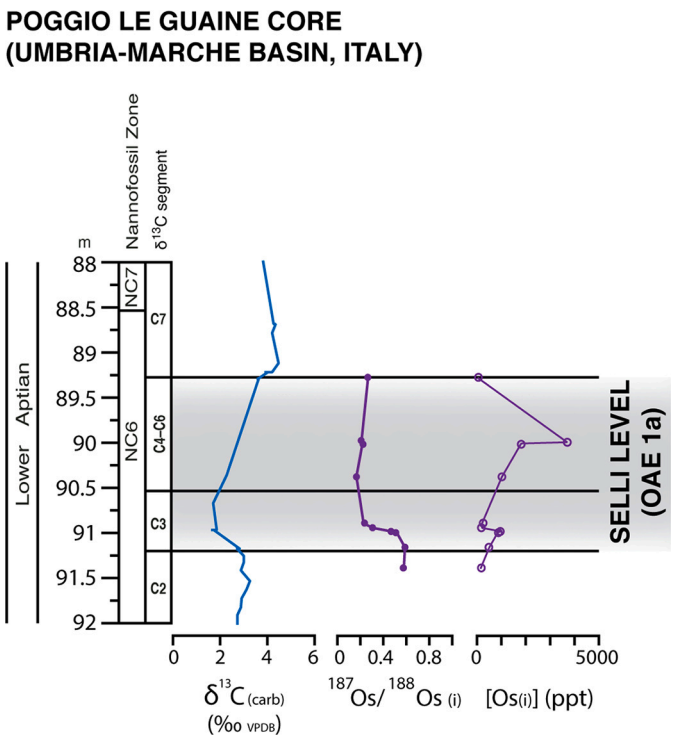

Fig. 3. Stratigraphic correlation of δ^{13}C ratios, and recorded ^{187}Os/^{188}Os$_{(i)}$ and [Os$_{(i)}$] values at 120 Ma for the Poggio le Guaine (PLG) core. Stratigraphic scale is in metres. δ^{13}C values, biostratigraphy, and carbon-isotope segments are sourced as for Fig. 4; all osmium data are from this study. Grey shaded area indicates the stratigraphic extent of the Selli Level.

4.2. Hg concentration and Hg/TOC ratio data

At DSDP Site 463, there is a clear increase in Hg content from the average of 16.4 ppb below the Selli Level Equivalent to a mean of 101 ppb within it, with a first increase up to 168.5 ppb in C3 (625.28–623.96 mbsf) and a second peak up to 471.5 ppb in the C4–lowest C5 segments (622.22–620.10 mbsf), before returning to much lower (mean 18.4 ppb) values in sediments above the Selli Level Equivalent (Fig. 4A). By contrast, the TOC contents of DSDP Site 463 samples that were also measured for mercury are relatively consistent, and low: typically <0.5 wt%, apart from for three samples in the middle of the Selli Level Equivalent that have values close to or above 1 wt%. Interestingly, no sample measured in this study had TOC contents of 7–8 wt% as reported for some stratigraphic layers at DSDP Site 463 by previous works (see Section 2.1). Consequently, the two increases in Hg concentrations are largely reproduced by Hg/TOC ratios, with peaks up to 802 ppb/wt% and 689 ppb/wt% in C3 and lowest C5 strata, respectively (Fig. 4A). Crucially, both peaks greatly exceed the range of error of background samples, confirming that they do not result from analytical uncertainty. A small number of samples have a TOC content that is too low to confidently interpret Hg/TOC ratios (Hg/TOC ratios based on TOC contents <0.2 wt% are generally deemed unreliable due to the high percentage error in the TOC measurement: see Grasby et al., 2016). However, the inclusion or exclusion of these data does not greatly affect the recorded stratigraphic trends.

Hg concentrations in the Cismon core are extremely variable throughout the studied interval, ranging between 3.7 and 334 ppb with a number of peaks: either side of the Barremian–Aptian boundary (at 34.21 m and 27.85 m), within the C3 to C4 strata (~23 m), and again in the C6 segment between 19.87 and 18.83 m (Fig. 4B). TOC contents of samples below the Selli Level Equivalent are typically very low (only three samples exceed 0.2 wt%), resulting in highly variable Hg/TOC values between 113 and 1637 ppb/wt% that also show peaks either side of the Barremian–Aptian boundary, although interpreting these data is greatly hindered due to the normalisation by extremely low TOC contents. By contrast, the typically higher TOC contents within the Selli Level Equivalent result in generally lower, though still variable, ratios between 7.9 and 468 ppb/wt% (Fig. 4B). However, the C3–C4 peak in Hg concentrations is only reproduced by a two data-point peak in Hg/TOC, with no increase in Hg/TOC ratios in the C6 segment.

Similarly to the Cismon core, the PLG record features rather variable sedimentary Hg concentrations between 1.4 and 201 ppb, with a number of peaks below the Selli Level and another peak within the lower part of the C4–C6 strata within it (Fig. 4C). Concentrations across the Barremian–Aptian boundary and above the Selli Level are particularly low (averaging 9.9 ppb). TOC contents increase markedly from typically <0.5 wt% below the Selli Level to values in excess of 2 wt% within it; one sample reaching 10.7 wt% (Fig. 4C). The various peaks in Hg are maintained to some degree following normalisation against TOC, with three peaks of between 200 and 600 ppb/wt%: one at 93.8–93.6 m, a second at 92.2 m (both below the OAE 1a horizon), and finally at 90.4 m (lowest C4–C6 strata), albeit consisting of just one or two data points (Fig. 4C). However, it should be noted that several PLG Hg data points are normalised against low (but >0.2 wt%) TOC contents, creating a high level of uncertainty in the Hg/TOC stratigraphic trend. Many of the PLG Hg/TOC peaks do not significantly exceed this range of error; thus, they cannot be unambiguously interpreted as marking an external influx of mercury.

Hg concentrations are consistently low through most of the Notre-Dame-de-Rosans strata (averaging 28.6 ppb), apart from a peak up to 156.5 ppb (mean 60.0 ppb) spanning the uppermost C3, all of C4, and lower C5 segments (18.8–24.9 m; Fig. 4D). Newly measured TOC contents in the samples analyzed for mercury show comparable trends to those previously published by Giraud et al. (2018), averaging approximately 0.5 wt% throughout most of the studied record, except in the C6 upper part of the Selli Level Equivalent (the Niveau Goguel), where

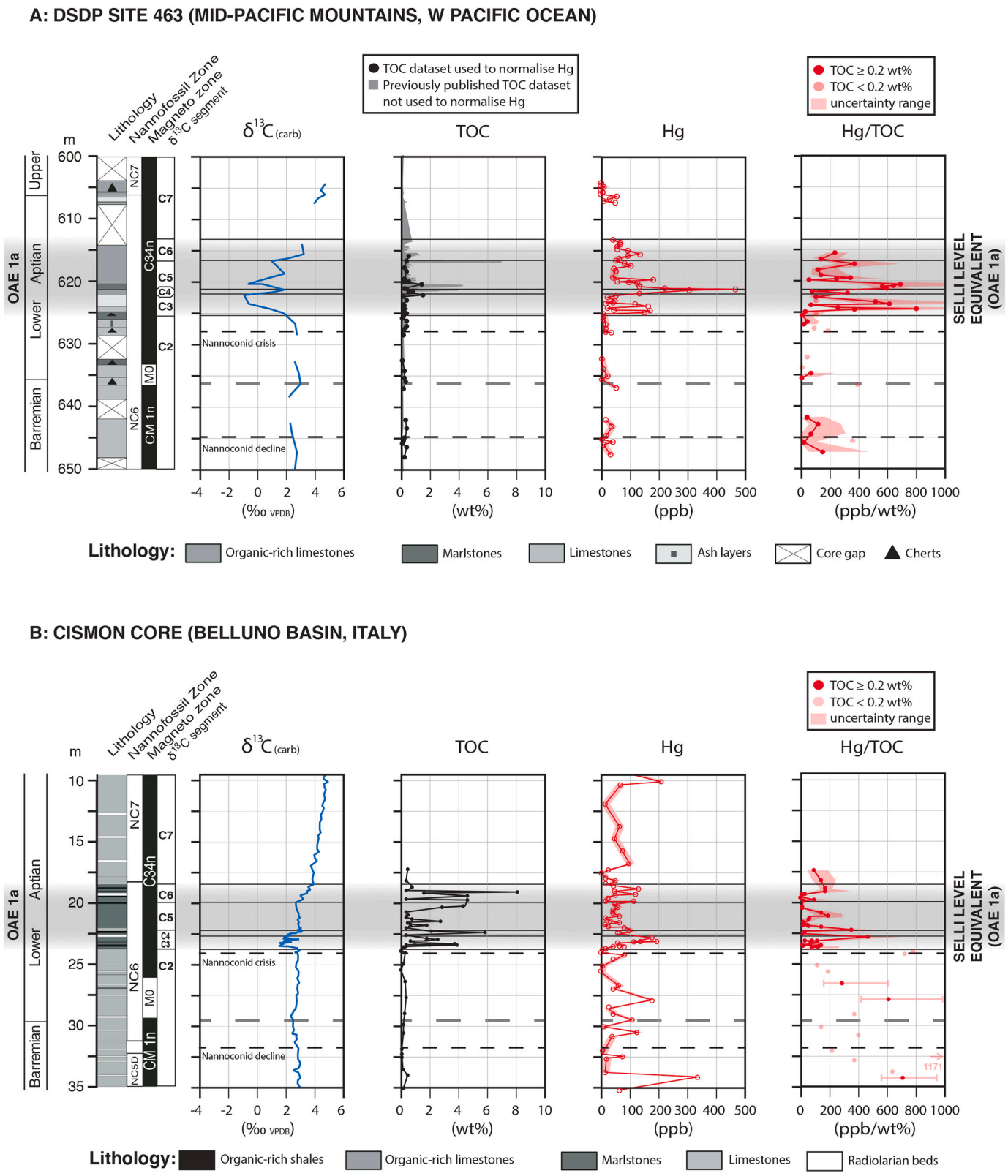

Fig. 4. Geochemical data plots for $\delta^{13}C$, TOC, Hg contents, and Hg/TOC ratios for DSDP Site 463, the Cismon core, Poggio le Guaine (PLG) core, Notre-Dame-de-Rosans, the DH-1 core, and Petrobras Well D. Semi-transparent Hg/TOC data points indicate Hg/TOC ratios based on TOC contents <0.2 wt% (below the limit of reliability recommended by Grasby et al., 2016). The ±15 ppb range of Hg concentration uncertainty is indicated on each Hg data plot by a pale red field; the ±0.1 wt % uncertainty on TOC measurements is not visible on this scale. The uncertainty range for each Hg/TOC value based on ±15 ppb Hg and ±0.1 wt% TOC is shown on each Hg/TOC plot by a pale red field. Grey shaded areas indicate the stratigraphic extent of the Selli Level (at PLG) or equivalent strata deposited during OAE 1a (all other sites), the grey dashed line the Barremian–Aptian boundary, and thin black dashed lines the recorded decline and crisis of nannoconids. All stratigraphic scales are in metres. All Hg and Hg/TOC data are new for this study. TOC data are sourced as follows: the DSDP Site 463, Poggio le Guaine core and Notre-Dame-de-Rosans from this study; the Cismon core from Bottini et al. (2012) and this study; the DH-1 core from Midtkandal et al. (2016); Petrobras Well D from Tedeschi et al. (2020).

$\delta^{13}C$ data and information on lithology, biostratigraphy, magnetostratigraphy, and carbon-isotope segmentation are sourced as follows: DSDP Site 463 from Tarduno et al. (1989), Erba (1994), Bottini et al. (2012), and Ando (2015); the Cismon core from Menegatti et al. (1998), Erba et al. (1999), Channell et al. (2000); the Poggio le Guaine core from Savian et al. (2016); Notre-Dame-de-Rosans from Giraud et al. (2018); DH-1 core from Midtkandal et al. (2016); Petrobras Well D from Tedeschi et al. (2020). Previously published TOC data for DSDP Site 463 and Notre-Dame-de-Rosans that were not used for normalisation of Hg are sourced from Bottini et al. (2012) and Giraud et al. (2018), respectively. The $\delta^{13}C$ and Hg data from DSDP Site 463 and the Cismon and DH-1 cores are presented alongside evidence for clay and pyrite/sulphur contents in Supplementary Fig. 2. (For interpretation of the references to colour in this figure legend, the reader is referred to the web version of this article.)

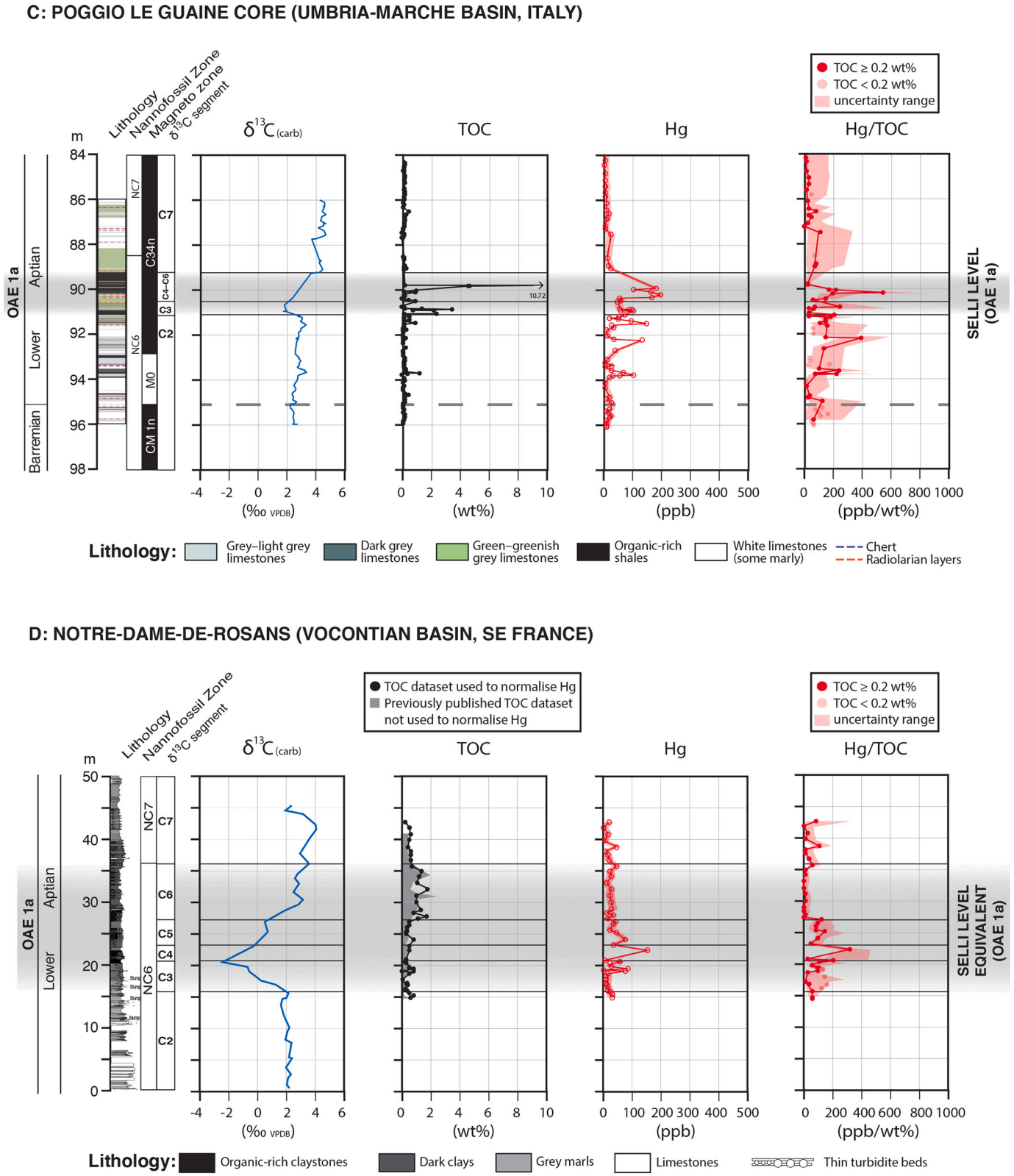

Fig. 4. (*continued*).

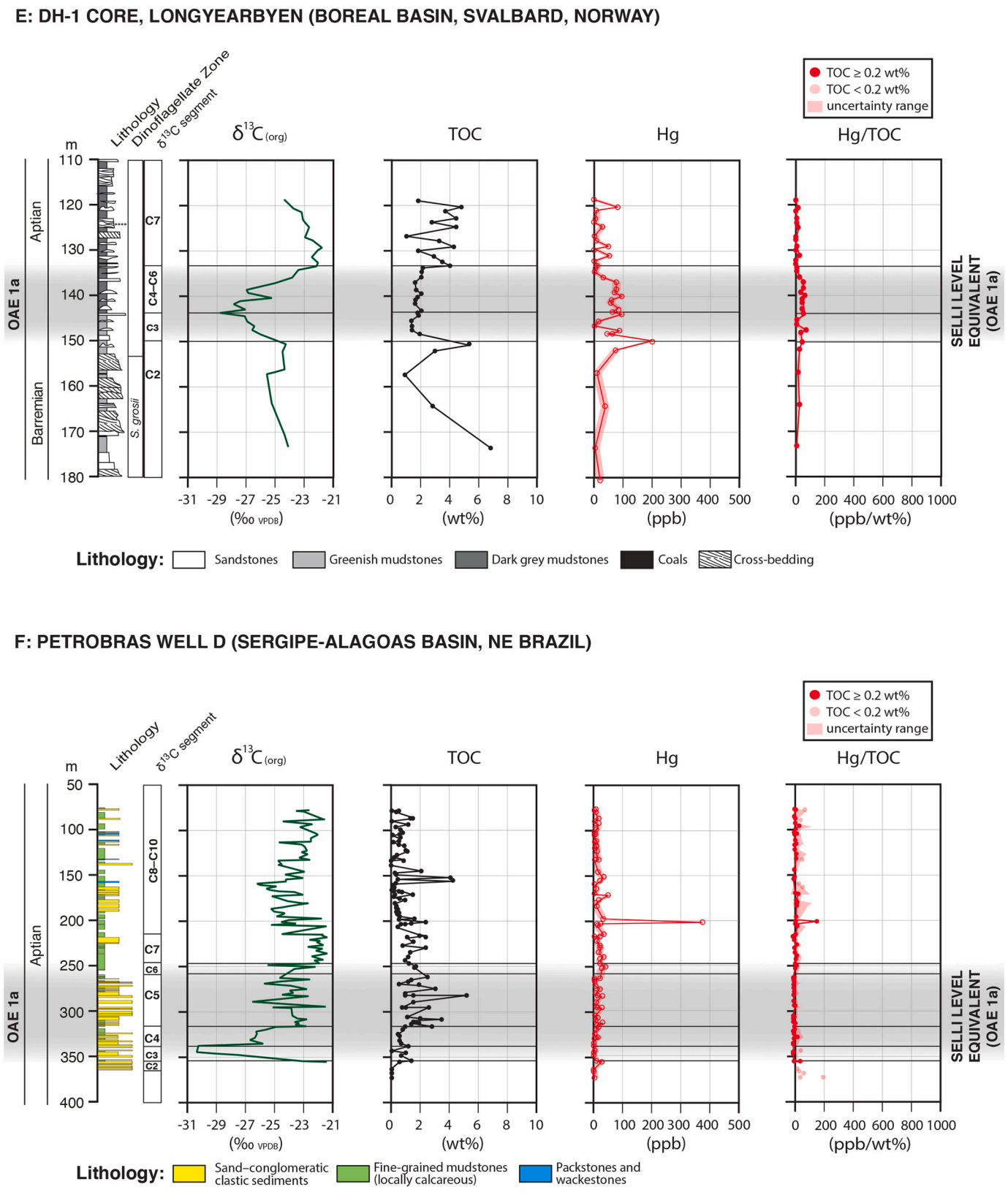

Fig. 4. (*continued*).

values rise to between 1 and 2 wt% (Fig. 4D). Consequently, the peak in Hg concentrations largely remains following normalisation by TOC, with an increase in Hg/TOC ratios up to 333 ppb/wt% in C4 strata, compared to consistently lower values averaging 64 ppb/wt% throughout the rest of the studied interval.

Hg concentrations are variable throughout the studied interval of the DH-1 core, but show a systematic increase across the Selli Level Equivalent. The basal (C3) strata are marked by a peak up to 202 ppb at 150.47 m, which is succeeded by a broader increase averaging 73.8 ppb across the upper C4–C6 segments (144.3–136.02 m), compared to much

lower contents that are typically <10 ppb throughout the rest of the record (Fig. 4E). When normalised against the TOC contents of these samples (previously published by Midtkandal et al., 2016), the C3 peak in Hg largely disappears, but the elevated Hg contents across C4–C6 strata are reflected by a rise in average Hg/TOC values to 40 ppb/wt% in these strata, compared to 12.1 ppb/wt% for the rest of the record (Fig. 4E).

Hg concentrations are consistently very low (averaging 13.9 ppb) throughout the studied interval of the Petrobras Well D, and show no increase across the postulated Selli Level Equivalent (Fig. 4F). As for the DH-1 core, TOC contents of these samples have been previously published (Tedeschi et al., 2020), with a marked increase from <0.1 wt% below the OAE 1a level to generally between 1 and 3 wt% (up to a maximum of 5.22 wt%) within it. Consequently, Hg/TOC ratios are generally also very low (averaging <20 ppb/wt%) with a few higher values near the base of the studied interval caused by low TOC contents (Fig. 4F). There is one sample (from 201.43 m) with anomalously high Hg concentrations and Hg/TOC ratios of 373 ppb and 158 ppb/wt%, respectively, but this is significantly above the top of the Selli Level Equivalent.

5. Discussion

5.1. Tethyan Hg-cycle disturbances prior to OAE 1a

Volcanic activity related to G-OJP emplacement has been previously proposed as having occurred during latest Barremian times, based on enrichments in mercury and other trace metals across the Barremian–Aptian boundary, especially in Tethyan stratigraphic archives (Erba et al., 2015; Charbonnier et al., 2018b). Some increase in submarine volcanism and/or basalt–seawater interaction might also be registered by a small shift towards mantle compositions in Pb and Os isotopes across the Barremian–Aptian boundaries of the Shatsky Rise and Cismon records, respectively (Kuroda et al., 2011; Bottini et al., 2012). It has been further suggested that this G-OJP volcanism contributed to the decline in nannoconid fauna during the Barremian–Aptian transition (Erba et al., 2015). Whilst Hg concentrations and Hg/TOC ratios are highly variable in pre-OAE 1a strata from the Cismon and PLG cores, peaks around the Barremian–Aptian boundary (and particularly strata of the magnetic chron CM0) might support a mercury-cycle disturbance in the northwest Tethyan region at that time (Fig. 4B–C). However, interpretation of the Hg/TOC ratios for both the Cismon and PLG cores is greatly hindered by the very low TOC contents of most samples (and attendant large range of uncertainty) from strata below the Selli Level or equivalent. Indeed, given the relatively low organic-matter and (in the case of Cismon) sulphur contents in Barremian–Aptian boundary sediments (Fig. 4B–C; Supplementary Fig. 2B), a lithological control on mercury deposition, whereby the element is associated with clay minerals, is likely for these strata. This conclusion is reinforced by the absence of Hg peaks in strata above the PLG Selli Level, when argillaceous layers (which make up much of the Selli Level and are interbedded with limestones beneath it) discontinue, leaving only calcareous lithologies.

Even if there were one or more Hg-cycle perturbations (volcanically stimulated or otherwise) in the Tethyan realm during the Barremian–Aptian transition prior to OAE 1a, there is no evidence that such phenomena were occurring outside of this region. Hg concentrations and Hg/TOC ratios remain relatively low throughout the (admittedly incomplete) strata below the Selli Level Equivalent at DSDP Site 463 (Fig. 4A). Given how proximal this Mid-Pacific Mountains site was to the G-OJP, if volcanism on that LIP were capable of dispersing sufficient Hg to reach the northwest Tethys, the expectation would be for it to be recorded in more proximal sedimentary records as well. Nor can the absence of Barremian–Aptian Hg enrichment at DSDP Site 463 be attributed to overprinting by excess TOC, as the Hg concentrations themselves largely remain low. Thus, whilst activity on the G-OJP during the latest Barremian is not discounted as the cause of the nannoconid decline, if the LIP was volcanically active at that time then it apparently did not perturb either the regional or global mercury cycle significantly. Volcanism on the north-eastern Tethyan margin has been suggested as a potential cause of Hg peaks in Valanginian sedimentary records from the northwest Tethys (Charbonnier et al., 2017), but there is no clear indication that such eruptions took place during latest Barremian to early Aptian times. Thus, without evidence of north-western Tethyan eruptions or G-OJP mercury emissions during the Barremian–Aptian transition, the Hg/TOC variations documented stratigraphically below the Selli Level (or equivalent strata) in the Cismon and PLG cores cannot be conclusively linked to volcanism.

5.2. Evidence for submarine G-OJP volcanism at the onset of OAE 1a

The shift in $^{187}Os/^{188}Os_{(i)}$ values towards unradiogenic compositions in basal Selli Level (C3) strata of the PLG core matches published Os-isotope stratigraphic trends from other sites in the Tethys and Pacific (Fig. 5). This similarity supports the commencement of intense LIP volcanism, or at least some form of basalt–seawater interaction, during the onset of OAE 1a. There is a clear correlation between the $^{187}Os/^{188}Os_{(i)}$ shift and the increased Hg and Hg/TOC values at DSDP Site 463; however, no such relationship is documented in the Cismon or PLG cores (Fig. 5). Whilst no $^{187}Os/^{188}Os_{(i)}$ data exist for the other six sites studied for mercury here and by Charbonnier and Föllmi (2017), it can be seen that, although most of those locales record some enrichment (s) in sedimentary mercury, none of them feature a clear peak in Hg and Hg/TOC in the C3 segment comparable to that in coeval strata of DSDP Site 463 (Fig. 4 and Supplementary Fig. 1).

Given that by far the clearest sedimentary mercury enrichment during the onset of OAE 1a is at DSDP Site 463, it is possible that this single-site peak results from a lithological change in that archive, such as increased clay content or burial with pyrite (c.f., Shen et al., 2020). Alternatively, it may reflect a local input of Hg from increased wildfire activity/runoff of terrestrial organic matter (c.f. Daga et al., 2016; Grasby et al., 2017; Them et al., 2019). However, the C3 Hg enrichment at DSDP Site 463 does not correlate with an increase in total clay or pyrite content (Supplementary Fig. 2A), ruling out an association between mercury and such phases, and thereby discounting lithological/redox changes as the cause of the Hg/TOC increase. Organic-matter oxidation/degradation has been reported from the DSDP Site 463 Aptian record, but van Breugel et al. (2007) noted that the sediments from the basal part of the Selli Level Equivalent are less thermally mature than the rock layers stratigraphically below and above, making it unlikely that the C3 Hg/TOC peak merely results from post-depositional TOC depletion (c.f., Charbonnier et al., 2020). Both marine and terrestrially derived organic matter are known to be present in Selli Level Equivalent sediments of DSDP Site 463, but an increased abundance in terrestrial material specifically in the C3 Segment has not been robustly established (Mélières et al., 1981; Dean et al., 1984; van Breugel et al., 2007).

Notably, however, the Hg and Hg/TOC increase at the base of the Selli Level Equivalent stratigraphically correlates with the appearance of abundant tuffaceous layers (Fig. 6). Thus, it is likely that the mercury peaks at DSDP Site 463 were caused by nearby volcanic activity proximal to the G-OJP. The correlation between Hg enrichments, tuffaceous layers, and recorded shift in $^{187}Os/^{188}Os_{(i)}$ ratios to unradiogenic compositions further suggests that all three could have been caused by the same volcanic process. Given that the volcanic activity that caused the shift in seawater Os-isotope ratios represented a six- to tenfold increase on pre-event background activity (Bauer et al., 2017), it is highly unlikely that the volcanism responsible for the recorded Hg enrichment and $^{187}Os/^{188}Os_{(i)}$ shift at DSDP Site 463, which appears to have occurred at least proximally to the G-OJP, can have been anything other than intense activity on that LIP. Moreover, given the intensity of this LIP volcanism, the fact that the mercury enrichment only appears in a

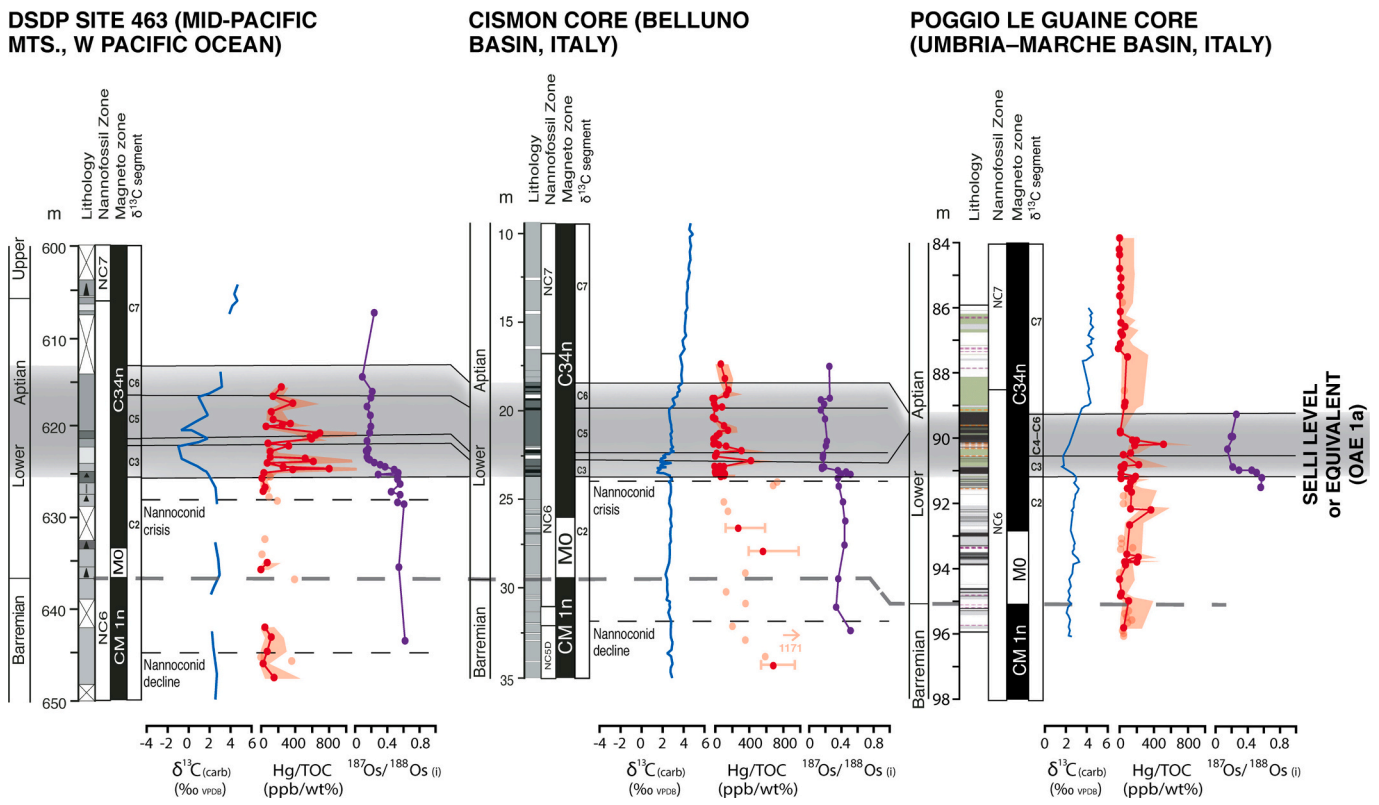

Fig. 5. Stratigraphic correlation of Hg/TOC ratios and $^{187}Os/^{188}Os_{(i)}$ trends from DSDP Site 463 and the Cismon and Poggio le Guaine (PLG) cores. Semi-transparent Hg/TOC data points indicate Hg/TOC ratios based on TOC contents <0.2 wt% (below the limit of reliability recommended by Grasby et al., 2016). The uncertainty range for each Hg/TOC value based on ±15 ppb Hg and ±0.1 wt% TOC is shown by the pale red field. Published Os data from DSDP Site 463 and the Cismon core are from Bottini et al. (2012); Poggio le Guaine Os data and all Hg data are from this study. Grey shaded areas indicate the stratigraphic extent of the Selli Level or equivalent OAE 1a strata, the grey dashed line the Barremian–Aptian boundary, and thin black dashed lines the recorded decline and crisis of nannoconids. All stratigraphic scales are in metres. Information on lithology, $\delta^{13}C$ values, biostratigraphy, magnetostratigraphy, and carbon-isotope segments are sourced as for Fig. 4. (For interpretation of the references to colour in this figure legend, the reader is referred to the web version of this article.)

site proximal to the G-OJP, and not correlative with $^{187}Os/^{188}Os_{(i)}$ shifts in the Tethyan realm, supports predominantly submarine eruptions, as also concluded by previous studies based on trends in other trace-element concentrations and lead-isotope signatures (Kuroda et al., 2011; Erba et al., 2015). The differing seawater residence times of osmium (10s kyr) and mercury (100s yr) would have enabled unradiogenic Os sourced from this volcanism to mix throughout the global ocean, whilst rapid Hg scavenging limited any evidence of a mercury flux to near the G-OJP, as documented in this study.

The slight possibility that the correlative Hg enrichment and $^{187}Os/^{188}Os_{(i)}$ shift at DSDP Site 463 were caused by HALIP volcanism is ruled out by the absence of a similar Hg peak in the C3 sediments of the Tethyan and (especially) DH-1 archives. It is possible that the one data-point Hg spike at the base of the C3 level in the DH-1 core represents a volcanic Hg flux from the HALIP that was then overprinted by excess TOC burial (as previously proposed for other sites by Percival et al., 2015, and Charbonnier and Föllmi, 2017), but this interpretation is speculative, and there is also no evidence for such an overprinting of increased Hg concentrations at any other site (Fig. 4 and Supplementary Fig. 1). If the HALIP had emitted sufficient mercury to the atmosphere to reach the Pacific, it is highly unlikely that there would be little clear record of such Hg output in any of the comparatively proximal Arctic or European/Tethyan sedimentary records (see Fig. 2). Thus, the G-OJP is more likely to have been the primary source of mercury to the Mid-Pacific Mountains (and unradiogenic osmium to the global ocean as a whole).

Despite an apparent lack of impact on the Hg cycle, it cannot be excluded that the HALIP (as well as other carbon sources such as methane clathrates; e.g., Jahren et al., 2001) still contributed to causing the global C-cycle perturbation associated with OAE 1a. Such a scenario would likely have relied upon HALIP magmatic sills intruding organic-rich sediments with a low Hg content, causing massive emissions of isotopically light carbon, but little mercury output. However, it is not currently known whether such lithologies exist around the HALIP sills. Moreover, this scenario is at odds with the documentation of Hg-cycle perturbations in stratigraphic records of several events linked with LIPs thought to have featured thermogenic volatile emissions (e.g., Percival et al., 2015, 2017; Jones et al., 2019; Shen et al., 2019b), and with preliminary investigations of carbon and mercury contents in shales intruded by LIP magmas in South Africa, which show clear evidence for remobilisation of both volatiles (Svensen et al., 2018). Therefore, it is more likely that the role played by the HALIP in initiating OAE 1a (if any) was minor compared to that of G-OJP activity.

5.3. *Volcanic vs terrestrial sources of Hg to marine environments after the onset of OAE 1a*

More plausibly, the widespread sedimentary Hg enrichments documented across C4 (or even the very uppermost C3) to C5 strata of seven out of nine OAE 1a sites studied here and by Charbonnier and Föllmi (2017) might have been triggered by a perturbation of the atmospheric mercury inventory following emissions of the element to the atmosphere from one or both of HALIP volcanism and sill intrusion of organic-rich shales. Given that subaerial LIP volcanism is thought to have emitted large volumes of Hg to the atmosphere at other times in Earth's history (e.g., Sanei et al., 2012; Percival et al., 2017, 2018; Grasby et al., 2019), similar eruptions on areas of the G-OJP that emerged above the sea surface could also have produced this effect. However, because the

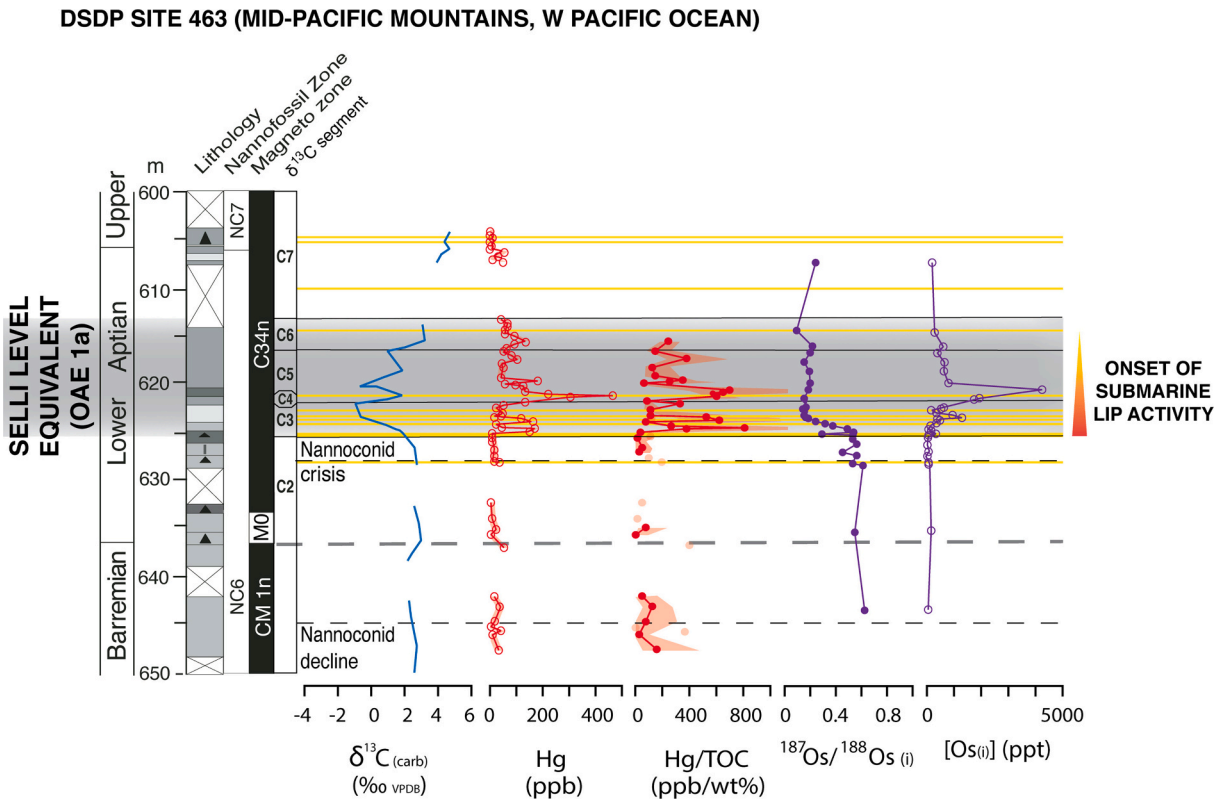

Fig. 6. Stratigraphic correlation of mercury concentrations, Hg/TOC ratios, and recorded $^{187}Os/^{188}Os_{(i)}$ and $[Os_{(i)}]$ values at 120 Ma for DSDP Site 463. Semi-transparent Hg/TOC data points indicate Hg/TOC ratios based on TOC contents <0.2 wt% (below the limit of reliability recommended by Grasby et al., 2016). Yellow lines mark the stratigraphic positions of tuffaceous layers (Thiede et al., 1981). The grey shaded area indicates the stratigraphic extent of Selli Level Equivalent sediments deposited during OAE 1a, the grey dashed line the Barremian–Aptian boundary, and thin black dashed lines the recorded decline and crisis of nannoconids. All stratigraphic scales are in metres. Information on lithology, $\delta^{13}C$ values, biostratigraphy, magnetostratigraphy, and carbon-isotope segments are sourced as for Fig. 4. The uncertainty range for each Hg and Hg/TOC value based on ±15 ppb Hg and ±0.1 wt% TOC are shown by the pale red field on their respective data plots. (For interpretation of the references to colour in this figure legend, the reader is referred to the web version of this article.)

C4–C5 strata postdate the onset of OAE 1a by on the order of 10s kyr (Li et al., 2008; Malinverno et al., 2010), the sedimentary Hg peaks might also result from lithological/redox changes or an increased input of terrigenous material following environmental responses to the climate disruption associated with the event.

As outlined in Section 1.3, mercury can be deposited in sediments bound to sulphides, particularly in euxinic water columns (Shen et al., 2020). In this context, the fact that the Cismon core records the development of euxinic conditions during OAE 1a (e.g., van Breugel et al., 2007), and that C4 (and C6) strata from that archive marked by increased Hg concentrations also feature elevated sulphur contents (Supplementary Fig. 2B), may indicate a switch to mercury burial with sulphides in the Belluno Basin during OAE 1a. If this association between Hg and S were the case, it could suggest that redox changes and pyrite-deposition controlled sedimentary Hg contents at that location during OAE 1a, rather than any external influx. And if so, it is likely that a similar situation existed for the PLG core, given the similar palaeoenvironments and Hg/TOC records of the Cismon and PLG records (only one or two high data points that do not exceed pre-event levels, or at least their range of uncertainty). Whilst this local redox/sulphide control on mercury for these two sites remains unproven, the relative paucity of high Hg/TOC values nonetheless means that robust evidence of a consistent external flux of mercury to the Belluno and Umbria-Marche basins during OAE 1a is currently lacking.

However, C4–C5 strata, specifically, of Notre-Dame-de-Rosans, La Bédoule, Glaise, and DSDP Site 463 record no evidence of euxinic conditions under which deposition of mercury with sulphides would have been most likely (Mélières et al., 1981; van Breugel et al., 2007; Westermann et al., 2013; Giraud et al., 2018), although DSDP Site 463 does feature an increased pyrite abundance in the C4 segment (Mélières et al., 1981). Euxinic conditions are extremely unlikely to have developed in the nearshore shallow-marine environment recorded by the DH-1 core, and a reasonably oxic (or at least not severely anoxic) setting is supported for that site by low sedimentary molybdenum and uranium concentrations, which show little or no enrichment above average-shale values except for two samples above the Selli Level Equivalent (*this study*; see Supplementary Fig. 2C). There is also no correlation between the C4–C5 Hg enrichments and abundance of clays/Al_2O_3 at any of DSDP Site 463, the DH-1 core, La Bédoule, or Glaise (see Supplementary Fig. 2, and Charbonnier and Föllmi, 2017). These trends support a lack of association between mercury and clay minerals in the C4–C5 strata at those sites, which would be expected due to the abundant TOC content in these same sediments, given the likely greater affinity of mercury for organic matter over clays when both phases are present (Shen et al., 2020). Thus, for at least four or five locations spanning the Arctic, Pacific, and north-western Tethyan realms presented here and in Charbonnier and Föllmi (2017), there is no evidence that mercury was deposited with a phase other than organic matter, making it likely that the C4–C5 peaks in Hg and Hg/TOC values were caused by an increased influx of mercury rather than lithological/redox changes.

Charcoal particles potentially indicative of wildfire activity have been reported from strata of Aptian age (Brown et al., 2012; Wang et al., 2019), although not from the Selli Level Equivalent specifically, or in any of the nine sites studied here and by Charbonnier and Föllmi (2017). Thus, there is no positive evidence that the widespread Hg influxes were the result of wildfires, although such a source cannot be completely ruled out. Nonetheless, terrestrially derived organic matter is abundant in the DH-1 core, and is thought to be present in some mixture with

marine material at all of DSDP Site 463, Notre-Dame-de-Rosans, and Glaise (van Breugel et al., 2007; Westermann et al., 2013; Midtkandal et al., 2016; Giraud et al., 2018). Organic-matter contents are too low at La Bédoule to reliably determine their composition. Thus, an increased input of terrigenous organic matter during a time of increased riverine runoff is a theoretically plausible source of the mercury to these sites during the early–middle part of OAE 1a, as previously proposed for the Early Jurassic Toarcian OAE (Them et al., 2019). However, peak weathering rates during OAE 1a are thought to have been during C3 rather than C4 (Tejada et al., 2009; Bottini et al., 2012; Lechler et al., 2015). Thus, if the mercury were derived from runoff of terrestrial material, an enrichment would be expected in the C3 segment rather than C4–C5 strata. Moreover, there is no evidence for an enhanced flux of mercury to the depositional setting of the Petrobras Well D core, despite an increase in the content of terrestrially derived organic matter in the upper part of the OAE 1a level (Tedeschi et al., 2020).

Consequently, whilst local terrestrial runoff cannot be discounted as the cause of the widespread C4–C5 Hg-cycle perturbations, LIP-related emissions of mercury to the atmosphere provide an equally plausible explanation. In the latter scenario, overprinting of Hg by excess TOC might have muted any record of Hg/TOC peaks at sites such as Cismon or PLG (see Charbonnier and Föllmi, 2017). As noted above, the lack of clear evidence of volcanic activity in the northwest Tethys during latest Barremian to early Aptian times means that local eruptions cannot be unambiguously stated as the cause of the observed C4–C5 Hg enrichments in Tethyan stratigraphic archives. Future studies incorporating mercury-isotope analyses may aid determination of the pathways taken by the element to reach depositional environments, and potentially indicate whether LIP activity or local processes such as terrestrial runoff and/or wildfires were the main cause of the widespread Hg enrichments recorded in the C4–C5 segments (c.f., Grasby et al., 2017; Them et al., 2019).

5.4. Implications for the impact of magmatic CO_2 emissions from LIPs on the global carbon cycle

Even if the widespread Hg-cycle disturbances during the early–middle (C4–C5) part of OAE 1a were related to subaerial volcanism and/or HALIP-related thermogenic volatile emissions, this activity apparently did not commence until after the onset of the event. Thus, it is unlikely that these processes played a major role in triggering the crisis. Instead, the combined Hg enrichments at DSDP Site 463 and lack of clear C3 peaks from elsewhere strongly support submarine volcanism on the G-OJP as the dominant form of LIP activity during the onset of OAE 1a, suggesting magmatic CO_2 output from that province as the main driver of the carbon-cycle perturbations that initiated climate change. Such a scenario supports the model of Bauer et al. (2017) that G-OJP mantle-carbon emissions were sufficient to cause the pronounced negative CIE documented in C3 strata that record the onset of OAE 1a.

However, it remains unclear whether G-OJP volcanism caused a global carbon-cycle perturbation simply due to the huge volume (59–77 $\times$ 10^6 km^3; Kerr and Mahoney, 2007), and high basaltic emplacement rate (possibly >100 km^3/yr; see introduction) of that LIP, particularly if it was combined with activity on the previously postulated twin province emplaced onto the Farallon Plate (Schlanger et al., 1981; Larson, 1991). If carbon emissions associated with the uniquely voluminous/rapid G-OJP magmatism were solely responsible for the negative CIE at the onset of OAE 1a, it would not detract from previous hypotheses that most (smaller) LIPs do not emit sufficient magmatic CO_2 to drive such disturbances unless combined with thermogenic volatiles and/or methane hydrate release (e.g., Hesselbo et al., 2000; Self et al., 2006). However, these results might also highlight the possibility that all LIPs can drive such disturbances through magmatic carbon emissions alone (as previously hypothesised by e.g., Saunders, 2016; Gutjahr et al., 2017). Further studies of (intrusive and extrusive) LIP basalts and sediments intruded by magmatic sills, both for the G-OJP, HALIP and other provinces, are needed in order to constrain the potential outputs of different volatile species from magmatic and thermogenic sources, and to determine the extent to which these different sources could have perturbed the cycling of different elements at the Earth's surface during different geological periods.

6. Conclusions

This study has investigated the influence of different magmatic processes related to the development of large igneous provinces (LIPs) on the global environment, using OAE 1a as a case study. By combining new mercury data for six records of that event, including the first sites studied outside of the Tethyan realm, and new osmium-isotope evidence from one of these six (Poggio le Guaine) with previously published datasets, the types of LIP activity likely to have been most prevalent during the onset and main body of the event have been determined.

Although osmium-isotope trends are broadly consistent across all new and previously studied sites in documenting intense LIP activity throughout OAE 1a, records of mercury-cycle disturbance show considerable geographical variability. The only unambiguous Hg perturbation during the onset of OAE 1a (matching Os-isotope evidence of LIP activity) is recorded in the Mid-Pacific Mountains very proximal to the Greater Ontong-Java Plateau (G-OJP). No such clear evidence for mercury-cycle perturbations at that time is recorded at Tethyan or South Atlantic sites, or from the Arctic region proximal to the High Arctic Large Igneous Province (HALIP). This pattern supports G-OJP volcanism as the dominant form of LIP activity at the onset of OAE 1a, causing the globally documented Os-isotope shift but only localized Hg enrichment. These findings also re-emphasise previous hypotheses that oceanic LIPs only influence mercury cycling in immediately proximal regions, due to the limited dispersal range of Hg emitted by submarine volcanism and other subaqueous basalt–seawater interactions, and likely do not cause a global-scale perturbation.

Crucially, whilst submarine LIP activity on the G-OJP during the onset of OAE 1a is clearly documented by osmium-isotope and mercury evidence, there is no clear indication for HALIP magmatism at that time. More widespread, if generally less pronounced, mercury-cycle perturbations appear to have taken place during the early–middle (C4–C5) part of OAE 1a. These disturbances could have been linked to a transient pulse in subaerial eruptions or thermogenic emissions related to the emplacement of the HALIP, or an intensification of/switch to subaerial eruptions on the G-OJP. However, a non-volcanic cause of these widespread Hg-cycle disturbances after the onset of OAE 1a, resulting from local environmental degradation during the event, cannot be ruled out. Even if these widespread mercury enrichments do signify subaerial LIP activity, the observation that they are not recorded globally in sediments that mark the onset of OAE 1a strongly suggests that such processes could not have caused the event. Instead, the results appear to confirm that submarine volcanism active on the Greater Ontong-Java Plateau, rather than sill intrusions of organic-rich sediments by the High Arctic LIP, was likely the primary trigger for OAE 1a.

Declaration of Competing Interest

The authors declare that they have no known competing financial interests or personal relationships that could have appeared to influence the work reported in this paper.

Acknowledgements

We greatly appreciate feedback from J.M. Castro and one anonymous reviewer that has improved this manuscript. We gratefully acknowledge John Farmer and the University of Edinburgh for provision of geochemical standard material, Stéphane Reboulet for fieldwork assistance at the Notre-Dame-de-Rosans section, and Steve Wyatt for aiding laboratory analyses. The Poggio le Guaine (PLG) core drilling was

financially supported by the Fundação de Apoio à Universidade de São Paulo and Petrobras grant 2405. Peter Szatmari is thanked for conducting the logistical arrangements required to perform rhenium-osmium analyses on PLG samples at the University of Alberta. The UNIS CO2 Lab is thanked for providing access to the DH-1 core samples, and we greatly appreciate assistance from Sverre Planke, Ivar Midtkandal, and Stéphane Polteau in sampling the core. We thank the UK Natural Environment Research Council (NERC) grant NE/G01700X/1 (to Tamsin Mather), the European Research Council consolidator grant ERC-2018-COG-B18717-V-ECHO (to Tamsin Mather), NERC PhD studentship NE/L501530/1 (to Lawrence Percival), the Flanders Research Foundation (FWO) grant no. 12P4519N (to Lawrence Percival), the MIURPRIN (Ministero dell'Istruzione, dell'Università e della Ricerca–-Progetti di Ricerca di Interesse Nazionale): grant no. PRIN 2017RX9XXXY to Elisabetta Erba, the Research Council of Norway Centres of Excellence (Project 223272 to Henrik Svensen), Petrobras (for financial support of the PLG and Petrobras Well D analyses and doctoral student funding for Leonardo R. Tedeschi), the Vrije Universiteit Brussel, and the Leverhulme Trust for funding.

Appendix A. Supplementary data

Supplementary data to this article can be found online at https://doi.org/10.1016/j.gloplacha.2021.103461.

References

Adloff, M., Greene, S.E., Parkinson, I.J., Naafs, B.D.A., Preston, W., Ridgwell, A., Lunt, D. J., Castro, J.M., Monteiro, F.M., 2020. Unravelling the sources of carbon emissions at the onset of Oceanic Anoxic Event (OAE) 1a. Earth Planet. Sci. Lett. 530, 115947. https://doi.org/10.1016/j.epsl.2019.115947.

Allègre, C.J., Birck, J.L., Capmas, F., Courtillot, V., 1999. Age of the Deccan traps using ^{187}Re–^{187}Os systematics. Earth Planet. Sci. Lett. 170, 197–204. https://doi.org/10.1016/S0012-821X(99)00110-7.

Ando, A., 2015. Intersite discrepancy in the amplitude of marine negative $\delta^{13}C$ excursion at the onset of early Aptian oceanic anoxic event 1a: reconciliation through Sr isotopic screening of peculiar diagenetic overprint on the Pacific reference section (Deep Sea Drilling Project Site 463). In: Neal, C.R., Sager, W.W., Sano, T., Erba, E. (Eds.), The Origin, Evolution, and Environmental Impact of Oceanic Large Igneous Provinces, Geological Society of America Special Paper, 511, pp. 329–339. https://doi.org/10.1130/2015.2511(17).

Ando, A., Kaiho, K., Kawahata, H., Kakegawa, T., 2008. Timing and magnitude of early Aptian extreme warming: Unraveling primary $\delta^{18}O$ variation in indurated pelagic carbonates at Deep Sea Drilling Project Site 463, central Pacific Ocean. Palaeogeogr. Palaeoclimatol. Palaeoecol. 260, 463–476. https://doi.org/10.1016/j.palaeo.2007.12.007.

Ando, T., Sawada, K., Takashima, R., Nishi, H., 2013. Paleoproductivity of dinoflagellate and cyanobacteria during the mid-Cretaceous oceanic anoxic events in the Vocontian Basin, SE France. In: 26th IMOG Organic Geochemistry: Trends for the 21st Century, 2, pp. 330–331.

Bagnato, E., Aiuppa, A., Parello, F., Calabrese, S., D'Alessandro, W., Mather, T.A., McGonigle, A.J.S., Pyle, D.M., Wängberg, I., 2007. Degassing of gaseous (elemental and reactive) and particulate mercury from Mount Etna volcano (Southern Italy). Atmos. Environ. 41, 7377–7388. https://doi.org/10.1016/j.atmosenv.2007.05.060.

Baudin, F., Fiet, N., Coccioni, R., Galeotti, S., 1998. Organic matter characterisation of the Selli Level (Umbria-Marche Basin, central Italy). Cretac. Res. 19, 701–714. https://doi.org/10.1006/cres.1998.0126.

Bauer, K.W., Zeebe, R.E., Wortmann, U.G., 2017. Quantifying the volcanic emissions which triggered Oceanic Anoxic Event 1a and their effect on ocean acidification. Sedimentology 64, 204–214. https://doi.org/10.1111/sed.12335.

Behar, F., Beaumont, V., de Penteado, H.L., 2001. Rock-Eval 6 technology: performances and developments. Oil Gas Sci. Technol. 56, 111–134. https://doi.org/10.2516/ogst:2001013.

Bond, D.P.G., Wignall, P.B., 2014. Large igneous provinces and mass extinctions: an update. In: Keller, G., Kerr, A.C. (Eds.), Volcnanism, Impacts, and Mass Extinctions: Causes and Effects, Geological Society of America Special Papers, 505, pp. SPE505–02. https://doi.org/10.1130/2014.2505(02).

Bottini, C., Cohen, A.S., Erba, E., Jenkyns, H.C., Coe, A.L., 2012. Osmium-isotope evidence for volcanism, weathering, and ocean mixing during the early Aptian OAE 1a. Geology 40, 583–586. https://doi.org/10.1130/G33140.1.

Bottini, C., Erba, E., Tiraboschi, D., Jenkyns, H.C., Schouten, S., Sinninghe Damsté, J.S., 2015. Climate variability and ocean fertility during the Aptian Stage. Clim. Past 11, 383–402. https://doi.org/10.5194/cp-11-383-2015.

Bowman, K.L., Hammerschmidt, C.R., Lamborg, C.H., Swarr, G., 2015. Mercury in the North Atlantic Ocean: the U.S. GEOTRACERS zonal and meridional sections. Deep Sea Res. II 116, 251–261. https://doi.org/10.1016/j.dsr2.2014.07.004.

Bralower, T.J., Arthur, M.A., Leckie, R.M., Sliter, W.V., Allard, D.J., Schlanger, S.O., 1994. Timing and paleoceanography of oceanic dysoxia/anoxia in the Late Barremian to Early Aptian (Early Cretaceous). Palaios 335–369. https://doi.org/10.2307/3515055.

Bréhéret, J.G., 1997. L'Aptien et l'Albien de la fosse vocontienne (des bordures au bassin): Evolution de la sédimentation et enseignements sur les événements anoxiques, 25. Société Géologique du Nord Publication (614 pp.).

Bréhéret, J.G., 1998. Episodes de sédimentation riche en matière organique dans les marnes bleues d'âge aptien et albien de la partie pélagique du bassin vocontien. Bull. Soc. Géol. France 4, 349–356. https://doi.org/10.2113/gssgfbull.IV.2.349.

Brown, S.A.E., Scott, A.C., Glasspool, I.J., Collinson, M.E., 2012. Cretaceous wildfires and their impact on the Earth system. Cretac. Res. 36, 162–190. https://doi.org/10.1016/j.cretres.2012.02.008.

Caillaud, A., Quijada, M., Huet, B., Reynaud, J.Y., Riboulleau, A., Bout-Roumazeilles, V., Baudin, F., Chappaz, A., Adatte, T., Ferry, J.N., Tribovillard, N., 2020. Turbidite-induced re-oxygenation episodes of the sediment-water interface in a diverticulum of the Tethys Ocean during the Oceanic Anoxic Event 1a: the French Vocontian Basin. Deposit. Rec. 6, 352–382. https://doi.org/10.1002/dep2.102.

Chaboureau, A.C., Guillocheau, F., Robin, C., Rohais, S., Moulin, M., Aslanian, D., 2013. Paleogeographic evolution of the central segment of the South Atlantic during Early Cretaceous times: paleotopographic and geodynamic implications. Tectonophysics 604, 191–223. https://doi.org/10.1016/j.tecto.2012.08.025.

Chambers, L.M., Pringle, M.S., Fitton, J.G., 2004. Phreatomagmatic eruptions on the Ontong Java Plateau: an Aptian $^{40}Ar/^{39}Ar$ age for volcaniclastic rocks at ODP Site 1184. In: Fitton, J.G., Mahoney, J.J., Wallace, P.J., Saunders, A.D. (Eds.), Origin and Evolution of the Ontong Java Plateau, Geological Society of London, Special Publications, 229, pp. 325–331. https://doi.org/10.1144/GSL.SP.2004.229.01.18.

Channell, J.E.T., Erba, E., Muttoni, G., Tremolada, F., 2000. Early Cretaceous magnetic stratigraphy in the APTICORE drill core and adjacent outcrop at Cismon (Southern Alps, Italy), and correlation to the proposed Barremian-Aptian boundary stratotype. Geol. Soc. Am. Bull. 112, 1430–1443. https://doi.org/10.1130/0016-7606(2000)112<1430:ECMSIT>2.0.CO;2.

Charbonnier, G., Föllmi, K.B., 2017. Mercury enrichments in lower Aptian sediments support the link between Ontong Java large igneous province activity and oceanic anoxic episode 1a. Geology 45, 63–66. https://doi.org/10.1130/G38207.1.

Charbonnier, G., Morales, C., Duchamp-Alphonse, S., Westermann, S., Adatte, T., Föllmi, K.B., 2017. Mercury enrichment indicates volcanic triggering of Valanginian environmental change. Sci. Rep. 7 https://doi.org/10.1038/srep40808.

Charbonnier, G., Adatte, T., Spangenberg, J.E., Föllmi, K.B., 2018a. The expression of early Aptian to latest Cenomanian oceanic anoxic events in the sedimentary record of the Briançonnais domain. Glob. Planet. Chang. 170, 76–92. https://doi.org/10.1016/j.gloplacha.2018.08.009.

Charbonnier, G., Godet, A., Bodin, S., Adatte, T., Föllmi, K.B., 2018b. Mercury anomalies, volcanic pulses, and drowning episodes along the northern Tethyan margin during the latest Hauterivian-earliest Aptian. Palaeogeogr. Palaeoclimatol. Palaeoecol. 505, 337–350. https://doi.org/10.1016/j.palaeo.2018.06.013.

Charbonnier, G., Adatte, T., Föllmi, K.B., Suan, G., 2020. Effect of intense weathering and post-depositional degradation of organic matter on Hg/TOC proxy in organic-rich sediments and its implications for deep-time investigations. Geochem. Geophys. Geosyst. 21 https://doi.org/10.1029/2019GC008707.

Coccioni, R., Nesci, O., Tramontana, M., Wezel, F.C., Moretti, E., 1987. Descrizione di un livello-guida "radiolaritico-bituminoso-ittiolitico" alla base delle Marne a Fucoidi nell'Appennino umbro-marchigiano. Boll. della Soc. Geol. Ital. 106, 183–192.

Coccioni, R., Franchi, R., Nesci, O., Perilli, N., Wezel, F.C., Battistini, F., 1990. Stratigrafia, micropaleontologia e mineralogia delle Marne a Fucoidi delle sezioni di Poggio le Guaine e del Fiume Bosso (Appennino umbro-marchigiano). Atti 2° Convegno Internazionale "Fossili, Evoluzione, Ambiente", Pergola, 25-30 ottobre 1987. Tecnostampa 163–201.

Coccioni, R., Jovane, L., Bancalà, G., Bucci, C., Fauth, G., Frontalini, F., Janikian, L., Savian, J., Paes de Almeida, R., Mathias, G.L., Ferreira da Trindade, I.R., 2012. Umbria-Marche Basin, Central Italy: a reference section for the Aptian-Albian interval at low latitudes. Sci. Drill. 13, 42–46. https://doi.org/10.2204/iodp.sd.13.07.2011.

Cogné, J.P., Humler, E., 2006. Trends and rhythms in global seafloor generation rate. Geochem. Geophys. Geosyst. 7 https://doi.org/10.1029/2005GC001148.

Cohen, A.S., Coe, A.L., 2002. New geochemical evidence for the onset of volcanism in the Central Atlantic magmatic province and environmental change at the Triassic-Jurassic boundary. Geology 30, 267–270. https://doi.org/10.1130/0091-7613(2002)030<0267:NGEFTO>2.0.CO;2.

Cohen, A.S., Coe, A.L., Bartlett, J.M., Hawkesworth, C.J., 1999. Precise Re-Os ages of organic-rich mudrocks and the Os isotope composition of Jurassic seawater. Earth Planet. Sci. Lett. 167, 159–173. https://doi.org/10.1016/S0012-821X(99)00026-6.

Corfu, F., Polteau, S., Planke, S., Faleide, J.I., Svensen, H., Zayoncheck, A., Stolbov, N., 2013. U–Pb geochronology of Cretaceous magmatism on Svalbard and Franz Josef Land, Barents Sea large igneous province. Geol. Mag. 150, 1127–1135. https://doi.org/10.1017/S0016756813000162.

Cumming, V.M., Poulton, S.W., Rooney, A.D., Selby, D., 2013. Anoxia in the terrestrial environment during the late Mesoproterozoic. Geology 41, 583–586. https://doi.org/10.1130/G34299.1.

Daga, R., Guevara, S.R., Pavlin, M., Rizzo, A., Lojen, S., Vreča, P., Horvat, M., Arribére, M., 2016. Historical records of mercury in southern latitudes over 1600 years: Lake Futalaufquen, Northern Patagonia. Sci. Total Environ. 553, 541–550. https://doi.org/10.1016/j.scitotenv.2016.02.114.

Dean, W.E., Claypool, G.E., Thide, J., 1984. Accumulation of organic matter in Cretaceous oxygen-deficient depositional environments in the central Pacific Ocean. Org. Geochem. 7, 39–51. https://doi.org/10.1016/0146-6380(84)90135-9.

Dickson, A.J., Cohen, A.S., Coe, A.L., Davies, M., Shcherbinina, E.A., Gavrilov, Y.O., 2015. Evidence for weathering and volcanism during the PETM from Arctic and Peri-

Tethys osmium isotope records. Palaeogeogr. Palaeoclimatol. Palaeoecol. 438, 300–307. https://doi.org/10.1016/j.palaeo.2015.08.019.
Dockman, D.M., Pearson, D.G., Heaman, L.M., Gibson, S.A., Sarkar, C., 2018. Timing and origin of magmatism in the Sverdrup Basin, Northern Canada—Implications for lithospheric evolution in the High Arctic Large Igneous Province (HALIP). Tectonophysics 742, 50–65. https://doi.org/10.1016/j.tecto.2018.05.010.
Dumitrescu, M., Brassell, S.C., 2006. Compositional and isotopic characteristics of organic matter for the early Aptian Oceanic Anoxic Event at Shatsky Rise, ODP Leg 198. Palaeogeogr. Palaeoclimatol. Palaeoecol. 235, 168–191. https://doi.org/10.1016/j.palaeo.2005.09.028.
Erba, E., 1994. Nannofossils and superplumes: the early Aptian "nannoconid crisis". Paleoceanogr. 9, 483–501. https://doi.org/10.1029/94PA00258.
Erba, E., 2004. Calcareous nannofossils and Mesozoic oceanic anoxic events. Mar. Micropaleontol. 52, 85–106. https://doi.org/10.1016/j.marmicro.2004.04.007.
Erba, E., Larson, R.L., 1998. The Cismon APTICORE (Southern Alps, Italy): a" reference section" for the Lower Cretaceous at low latitudes. Riv. Ital. Paleontol. Stratigr. 104, 181–192.
Erba, E., Tremolada, F., 2004. Nannofossil carbonate fluxes during the Early Cretaceous: Phytoplankton response to nutrification episodes, atmospheric CO_2, and anoxia. Paleoceanography 19. https://doi.org/10.1029/2003PA000884.
Erba, E., Channell, J.E.T., Claps, M., Jones, C., Larson, R., Opdyke, B., Premoli Silva, I., Riva, A., Salvini, G., Torricelli, S., 1999. Integrated stratigraphy of the Cismon Apticore (southern Alps, Italy); a "reference section" for the Barremian-Aptian interval at low latitudes. J. Foraminifer. Res. 29, 371–391.
Erba, E., Bottini, C., Weissert, H.J., Keller, C.E., 2010. Calcareous nannoplankton response to surface-water acidification around Oceanic Anoxic Event 1a. Science 329, 428–432. https://doi.org/10.1126/science.1188886.
Erba, E., Duncan, R.A., Bottini, C., Tiraboschi, D., Weissert, H., Jenkyns, H.C., Malinverno, A., 2015. Environmental consequences of Ontong Java Plateau and Kerguelen Plateau volcanism. In: Neal, C.R., Sager, W.W., Sano, T., Erba, E. (Eds.), The Origin, Evolution, and Environmental Impact of Oceanic Large Igneous Provinces, Geological Society of America Special Paper, 511, pp. 271–303. https://doi.org/10.1130/2015.2511(15).
Ericksen, J.A., Gustin, M.S., Schorran, D.E., Johnson, D.W., Lindberg, S.E., Coleman, J.S., 2003. Accumulation of atmospheric mercury in forest foliage. Atmos. Environ. 37, 1613–1622. https://doi.org/10.1016/S1352-2310(03)00008-6.
Finlay, A.J., Selby, D., Gröcke, D.R., 2010. Tracking the Hirnantian glaciation using Os isotopes. Earth Planet. Sci. Lett. 293, 339–348. https://doi.org/10.1016/j.epsl.2010.02.049.
Föllmi, K.B., Godet, A., Bodin, S., Linder, P., 2006. Interactions between environmental change and shallow water carbonate buildup along the northern Tethyan margin and their impact on the Early Cretaceous carbon isotope record. Paleoceanography 21. https://doi.org/10.1029/2006PA001313.
Gales, E., Black, B., Elkins-Tanton, L.T., 2020. Carbonatites as a record of the carbon isotope composition of large igneous province outgassing. Earth Planet. Sci. Lett. 535, 116076. https://doi.org/10.1016/j.epsl.2020.116076.
Giraud, F., Pittet, B., Grosheny, D., Baudin, F., Lécuyer, C., Sakamoto, T., 2018. The palaeoceanographic crisis of the Early Aptian (OAE 1a) in the Vocontian Basin (SE France). Palaeogeogr. Palaeoclimatol. Palaeoecol. 511, 483–505. https://doi.org/10.1016/j.palaeo.2018.09.014.
Gladczenko, T.P., Coffin, M.F., Eldholm, O., 1997. Crustal structure of the Ontong Java Plateau: modeling of new gravity and existing seismic data. J. Geophys. Res. 102, 22711–22729. https://doi.org/10.1029/97JB01636.
Grasby, S.E., Beauchamp, B., Bond, D.P.G., Wignall, P.B., Sanei, H., 2016. Mercury anomalies associated with three extinction events (Capitanian crisis, latest Permian extinction and the Smithian/Spathian extinction) in NW Pangea. Geol. Mag. 153, 285–297. https://doi.org/10.1017/S0016756815000436.
Grasby, S.E., Wenjie, S., Yin, R., Gleason, J.D., Blum, J.D., Lepak, R.F., Hurley, J.P., Beauchamp, B., 2017. Isotopic signatures of mercury contamination in latest Permian oceans. Geology 45, 55–58. https://doi.org/10.1130/G38487.1.
Grasby, S.E., Them, T.R., Chen, Z., Yin, R., Ardakani, O.H., 2019. Mercury as a proxy for volcanic emissions in the geologic record. Earth Sci. Rev. 196, 102880. https://doi.org/10.1016/j.earscirev.2019.102880.
Gröcke, D.R., Hesselbo, S.P., Jenkyns, H.C., 1999. Carbon-isotope composition of Lower Cretaceous fossil wood: Ocean-atmosphere chemistry and relation to sea-level change. Geology 27, 155–158. https://doi.org/10.1130/0091-7613(1999)027<0155:CICOLC>2.3.CO;2.
Gutjahr, M., Ridgwell, A., Sexton, P.F., Anagnostou, E., Pearson, P.N., Pälike, H., Norris, R.D., Thomas, E., Foster, G.L., 2017. Very large release of mostly volcanic carbon during the Palaeocene–Eocene Thermal Maximum. Nature 548, 573–577. https://doi.org/10.1038/nature23646.
Hammer, Ø., Jones, M.T., Schneebeli-Hermann, E., Hansen, B.B., Bucher, H., 2019. Are Early Triassic extinction events associated with mercury anomalies? A reassessment of the Smithian/Spathian boundary extinction. Earth Sci. Rev. 195, 179–190. https://doi.org/10.1016/j.earscirev.2019.04.016.
Hein, J.R., Vanek, E., 1981. Origin and alteration of volcanic ash and pelagic brown clay, Deep Sea Drilling Project Leg 62, north-central Pacific. In: Initial Reports of the Deep Sea Drilling Project, 62, pp. 559–569. https://doi.org/10.2973/dsdp.proc.62.120.1981.
Hesselbo, S.P., Gröcke, D.R., Jenkyns, H.C., Bjerrum, C.J., Farrimond, P., Morgans-Bell, H.S., Green, O.R., 2000. Massive dissociation of gas hydrate during a Jurassic oceanic anoxic event. Nature 406, 392–395. https://doi.org/10.1038/35019044.
Hibsch, C., Jandel, D., Montenat, C., Ott d'Estevou, P., 1992. Evénements tectoniques crétacés dans la partie méridionale du bassin subalpin (massif Ventoux-Lure et partie orientale de l'arc de Castellane, SE France). Implications géodynamiques. Bull. Soc. Géol. France 163, 147–158.
Hoernle, K., Hauff, F., van den Bogaard, P., Werner, R., Mortimer, N., Geldmacher, J., Garbe-Schönberg, D., Davy, B., 2010. Age and geochemistry of volcanic rocks from the Hikurangi and Manihiki oceanic Plateaus. Geochim. Cosmochim. Acta 74, 7196–7219. https://doi.org/10.1016/j.gca.2010.09.030.
Hönisch, B., Ridgwell, A., Schmidt, D.N., Thomas, E., Gibbs, S.J., Sluijs, A., Zeebe, R., Kump, L., Martindale, R.C., Greene, S.E., Kiessling, W., Ries, J., Zachos, J.C., Royer, D.L., Barker, S., Marchitto, T.M., Moyer, R., Pelejero, C., Ziveri, P., Foster, G.L., Williams, B., 2012. The geological record of ocean acidification. Science 335, 1058–1063. https://doi.org/10.1126/science.1208277.
Hu, X., Zhao, K., Yilmaz, I.O., Li, Y., 2012. Stratigraphic transition and palaeoenvironmental changes from the Aptian oceanic anoxic event 1a (OAE1a) to the oceanic red bed 1 (ORB1) in the Yenicesihlar section, central Turkey. Cretac. Res. 38, 40–51. https://doi.org/10.1016/j.cretres.2012.01.007.
Jahren, A.H., Arens, N.C., Sarmiento, G., Guerrero, J., Amundson, R., 2001. Terrestrial record of methane hydrate dissociation in the Early Cretaceous. Geology 29, 159–162. https://doi.org/10.1130/0091-7613(2001)029<0159:TROMHD>2.0.CO;2.
Jenkyns, H.C., 1988. The early Toarcian (Jurassic) anoxic event: stratigraphic, sedimentary, and geochemical evidence. Am. J. Sci. 288, 101–151. https://doi.org/10.2475/ajs.288.2.101.
Jenkyns, H.C., 1995. Carbon-isotope stratigraphy and paleoceanographic significance of the Lower Cretaceous shallow-water carbonates of Resolution Guyot, Mid-Pacific Mountains. In: Winterer, E.L., Sager, W.W., Firth, J.V., Sinton, J.M. (Eds.), Proceedings of the Ocean Drilling Program, Scientific Results, 143. Ocean Drilling Program, College Station, Texas, pp. 99–104. https://doi.org/10.2973/odp.proc.sr.143.213.1995.
Jenkyns, H.C., 2010. Geochemistry of oceanic anoxic events. Geochem. Geophys. Geosyst. 11 https://doi.org/10.1029/2009GC002788.
Jenkyns, H.C., 2018. Transient cooling episodes during Cretaceous Oceanic Anoxic Events with special reference to OAE 1a (Early Aptian). Philos. Trans. R. Soc. A Math. Phys. Eng. Sci. 376, 20170073 https://doi.org/10.1098/rsta.2017.0073.
Jones, C.E., Jenkyns, H.C., 2001. Seawater strontium isotopes, oceanic anoxic events, and seafloor hydrothermal activity in the Jurassic and Cretaceous. Am. J. Sci. 301, 112–149. https://doi.org/10.2475/ajs.301.2.112.
Jones, M.T., Percival, L.M.E., Stokke, E.W., Frieling, J., Mather, T.A., Riber, L., Schubert, B.A., Schultz, B., Tegner, C., Planke, S., Svensen, H., 2019. Mercury anomalies across the Palaeocene–Eocene Thermal Maximum. Clim. Past 15, 217–236. https://doi.org/10.5194/cp-15-217-2019.
Kendall, B., Creaser, R.A., Reinhard, C.T., Lyons, T.W., Anbar, A.D., 2015. Transient episodes of mild environmental oxygenation and oxidative continental weathering during the late Archean. Sci. Adv. 1, e1500777 https://doi.org/10.1126/sciadv.1500777.
Kerr, A.C., Mahoney, J.J., 2007. Oceanic plateaus: problematic plumes, potential paradigms. Chem. Geol. 241, 332–353. https://doi.org/10.1016/j.chemgeo.2007.01.019.
Kongchum, M., Hudnall, W.H., Delaune, R.D., 2011. Relationship between sediment clay minerals and total mercury. J. Environ. Sci. Health A 46, 534–539. https://doi.org/10.1080/10934529.2011.551745.
Koutsoukos, E.A.M., 1992. Late Aptian to Maastrichtian foraminiferal biogeography and palaeoceanography of the Sergipe Basin, Brazil. Palaeogeogr. Palaeoclimatol. Palaeoecol. 92, 295–324. https://doi.org/10.1016/0031-0182(92)90089-N.
Kuhnt, W., Holbourn, A., Moullade, M., 2011. Transient global cooling at the onset of early Aptian oceanic anoxic event (OAE) 1a. Geology 39, 323–326. https://doi.org/10.1130/G31554.1.
Kuroda, J., Tanimizu, M., Hori, R.S., Suzuki, K., Ogawa, N.O., Tejada, M.L.G., Coffin, M.F., Coccioni, R., Erba, E., Ohkouchi, N., 2011. Lead isotopic record of Barremian–Aptian marine sediments: Implications for large igneous provinces and the Aptian climatic crisis. Earth Planet. Sci. Lett. 307, 126–134. https://doi.org/10.1016/j.epsl.2011.04.021.
Larson, R.L., 1991. Latest pulse of Earth: evidence for a mid-Cretaceous superplume. Geology 19, 547–550. https://doi.org/10.1130/0091-7613(1991)019<0547:LPOEEF>2.3.CO;2.
Larson, R.L., Erba, E., 1999. Onset of the Mid-Cretaceous greenhouse in the Barremian-Aptian: igneous events and the biological, sedimentary, and geochemical responses. Paleoceanography 14. https://doi.org/10.1029/1999PA900040.
Lechler, M., Pogge von Strandmann, P.A.E., Jenkyns, H.C., Prosser, G., Parente, M., 2015. Lithium-isotope evidence for enhanced silicate weathering during OAE 1a (Early Aptian Selli event). Earth Planet. Sci. Lett. 432, 210–222. https://doi.org/10.1016/j.epsl.2015.09.052.
Li, Y.X., Bralower, T.J., Montañez, I.P., Osleger, D.A., Arthur, M.A., Bice, D.M., Herbert, T.D., Erba, E., Premoli Silva, I., 2008. Toward an orbital chronology for the early Aptian Oceanic Anoxic Event (OAE1a, ~120 Ma). Earth Planet. Sci. Lett. 271, 88–100. https://doi.org/10.1016/j.epsl.2008.03.055.
Lowrie, W., Alvarez, W., Premoli Silva, I., Monechi, S., 1980. Lower Cretaceous magnetic stratigraphy in Umbrian pelagic carbonate rocks. Geophys. J. Int. 60, 263–281. https://doi.org/10.1111/j.1365-246X.1980.tb04292.x.
Malinverno, A., Erba, E., Herbert, T.D., 2010. Orbital tuning as an inverse problem: Chronology of the early Aptian oceanic anoxic event 1a (Selli Level) in the Cismon APTICORE. Paleoceanogr. 25 https://doi.org/10.1029/2009PA001769.
McElwain, J.C., Wade-Murphy, J., Hesselbo, S.P., 2005. Changes in carbon dioxide during an oceanic anoxic event linked to intrusion into Gondwana coals. Nature 435, 479–482. https://doi.org/10.1038/nature03618.
Méhay, S., Keller, C.E., Bernasconi, S.M., Weissert, H., Erba, E., Bottini, C., Hochuli, P.A., 2009. A volcanic CO_2 pulse triggered the Cretaceous Oceanic Anoxic Event 1a and a biocalcification crisis. Geology 37, 819–822. https://doi.org/10.1130/G30100A.1.

Mélières, F., Deroo, G., Herbin, J.P., 1981. Organic-matter-rich and hypersiliceous Aptian sediments from western Mid-Pacific Mountains. In: Initial Reports of the Deep Sea Drilling Project, 62, pp. 903–915. https://doi.org/10.2973/dsdp.proc.62.146.1981.

Menegatti, A.P., Weissert, H., Brown, R.S., Tyson, R.V., Farrimond, P., Strasser, A., Caron, M., 1998. High-resolution $\delta^{13}C$ stratigraphy through the Early Aptian "Livello Selli" of the Alpine Tethys. Paleoceanography 13. https://doi.org/10.1029/98PA01793.

Midtkandal, I., Svensen, H., Planke, S., Corfu, F., Polteau, S., Torsvik, T.H., Faleide, J.I., Grundvåg, S.A., Selnes, H., Kürschner, W., Olaussen, S., 2016. The Aptian (Early Cretaceous) oceanic anoxic event (OAE1a) in Svalbard, Barents Sea, and the absolute age of the Barremian-Aptian boundary. Palaeogeogr. Palaeoclimatol. Palaeoecol. 463, 126–135. https://doi.org/10.1016/j.palaeo.2016.09.023.

Mutterlose, J., Bottini, C., Schouten, S., Sinninghe Damsté, J.S., 2014. High sea-surface temperatures during the early Aptian Oceanic Anoxic Event 1a in the Boreal Realm. Geology 42, 439–442. https://doi.org/10.1130/G35394.1.

Naafs, B.D.A., Pancost, R.D., 2016. Sea-surface temperature evolution across Aptian Oceanic Anoxic Event 1a. Geology 44, 959–962. https://doi.org/10.1130/G38575.1.

Naafs, B.D.A., Castro, J.M., De Gea, G.A., Quijano, M.L., Schmidt, D.N., Pancost, R.D., 2016. Gradual and sustained carbon dioxide release during Aptian Oceanic Anoxic Event 1a. Nat. Geosci. 9, 135–139. https://doi.org/10.1038/ngeo2627.

Neumann, E.R., Svensen, H., Tegner, C., Planke, S., Thirlwall, M., Jarvis, K.E., 2013. Sill and lava geochemistry of the mid-Norway and NE Greenland conjugate margins. Geochem. Geophys. Geosyst. 14 https://doi.org/10.1002/ggge.20224.

Pancost, R.D., Crawford, N., Magness, S., Turner, A., Jenkyns, H.C., Maxwell, J.R., 2004. Further evidence for the development of photic-zone euxinic conditions during Mesozoic oceanic anoxic events. J. Geol. Soc. 161, 353–364. https://doi.org/10.1144/0016764903-059.

Paquay, F.S., Ravizza, G., 2012. Heterogeneous seawater $^{187}Os/^{188}Os$ during the late Pleistocene glaciations. Earth Planet. Sci. Lett. 349, 126–138. https://doi.org/10.1016/j.epsl.2012.06.051.

Percival, L.M.E., Witt, M.L.I., Mather, T.A., Hermoso, M., Jenkyns, H.C., Hesselbo, S.P., Al-Suwaidi, A.H., Storm, M.S., Xu, W., Ruhl, M., 2015. Globally enhanced mercury deposition during the end-Pliensbachian extinction and Toarcian OAE: a link to the Karoo–Ferrar Large Igneous Province. Earth Planet. Sci. Lett. 428, 267–280. https://doi.org/10.1016/j.epsl.2015.06.064.

Percival, L.M.E., Ruhl, M., Hesselbo, S.P., Jenkyns, H.C., Mather, T.A., Whiteside, J.H., 2017. Mercury evidence for pulsed volcanism during the end-Triassic mass extinction. Proc. Natl. Acad. Sci. U. S. A. 114, 7929–7934. https://doi.org/10.1073/pnas.1705378114.

Percival, L.M.E., Jenkyns, H.C., Mather, T.A., Dickson, A.J., Batenburg, S.J., Ruhl, M., Hesselbo, S.P., Barclay, R., Jarvis, I., Robinson, S.A., Woelders, L., 2018. Does Large Igneous Province volcanism always perturb the mercury cycle? Comparing the records of Oceanic Anoxic Event 2 and the end-Cretaceous to other Mesozoic events. Am. J. Sci. 318, 799–860. https://doi.org/10.2475/08.2018.01.

Percival, L.M.E., Bergquist, B.A., Mather, T.A., Sanei, H., 2021. Sedimentary mercury enrichments as a tracer of Large Igneous Province volcanism. In: Ernst, R.E., Dickson, A.J., Bekker, A. (Eds.), Large Igneous Provinces: A Driver of Global Environmental and Biotic Change. AGU Geophysical Monograph, 255, pp. 247–262. https://doi.org/10.1002/9781119507444.ch11.

Peucker-Ehrenbrink, B., Jahn, B.M., 2001. Rhenium-osmium isotope systematics and platinum group element concentrations: loess and the upper continental crust. Geochem. Geophys. Geosyst. 2 https://doi.org/10.1029/2001GC000172.

Peucker-Ehrenbrink, B., Ravizza, G., 2000. The marine osmium isotope record. Terra Nova 12, 205–219. https://doi.org/10.1046/j.1365-3121.2000.00295.x.

Polteau, S., Hendriks, B.W.H., Planke, S., Ganerød, M., Corfu, F., Faleide, J.I., Midtkandal, I., Svensen, H., Myklebust, R., 2016. The Early Cretaceous Barents Sea Sill Complex: distribution, $^{40}Ar/^{39}Ar$ geochronology, and implications for carbon gas formation. Palaeogeogr. Palaeoclimatol. Palaeoecol. 441, 83–95. https://doi.org/10.1016/j.palaeo.2015.07.007.

Price, G.D., 2003. New constraints upon isotope variation during the early Cretaceous (Barremian–Cenomanian) from the Pacific Ocean. Geol. Mag. 140, 513–522. https://doi.org/10.1017/S0016756803008100.

Pyle, D.M., Mather, T.A., 2003. The importance of volcanic emissions for the global atmospheric mercury cycle. Atmos. Environ. 37, 5115–5124. https://doi.org/10.1016/j.atmosenv.2003.07.011.

Robinson, S.A., Clarke, L.J., Nederbragt, A., Wood, I.G., 2008. Mid-Cretaceous oceanic anoxic events in the Pacific Ocean revealed by carbon-isotope stratigraphy of the Calera Limestone, California, USA. Geol. Soc. Am. Bull. 120, 1416–1426. https://doi.org/10.1130/B26350.1.

Robinson, S.A., Heimhofer, U., Hesselbo, S.P., Petrizzo, M.R., 2017. Mesozoic climates and oceans – a tribute to Hugh Jenkyns and Helmut Weissert. Sedimentology 64, 1–15. https://doi.org/10.1111/sed.12349.

Sanei, H., Grasby, S.E., Beauchamp, B., 2012. Latest Permian mercury anomalies. Geology 40, 63–66. https://doi.org/10.1130/G32596.1.

Saunders, A.D., 2016. Two LIPs and two Earth-system crises: the impact of the North Atlantic Igneous Province and the Siberian Traps on the Earth-surface carbon cycle. Geol. Mag. 153, 201–222. https://doi.org/10.1017/S0016756815000175.

Savian, J., Trindade, R., Janikian, L., Jovane, L., de Almeida, R.P., Coccioni, R., Frontalini, F., Sideri, M., Figueiredo, M., Tedeschi, L.R., Jenkyns, H.C., 2016. The Barremian-Aptian boundary in the Poggio le Guaine core (central Italy): evidence for magnetic polarity Chron M0r and oceanic anoxic event 1a. In: Menichetti, M., Coccioni, R., Montanari, A. (Eds.), The Stratigraphic Record of Gubbio: Integrated Stratigraphy of the Late Cretaceous–Paleogene Umbria-Marche Pelagic Basin, Geological Society of America Special Paper, 524, pp. 57–78. https://doi.org/10.1130/2016.2524(05).

Scaife, J.D., Ruhl, M., Dickson, A.J., Mather, T.A., Jenkyns, H.C., Percival, L.M.E., Hesselbo, S.P., Cartwright, J., Eldrett, J.S., Bergman, S.C., Minisini, D., 2017. Sedimentary mercury enrichments as a marker for submarine large igneous province volcanism? Evidence from the mid-cenomanian event and oceanic anoxic event 2 (Late Cretaceous). Geochem. Geophys. Geosyst. 18 https://doi.org/10.1002/2017GC007153.

Schlanger, S.O., Jenkyns, H.C., 1976. Cretaceous oceanic anoxic events: causes and consequences. Geol. Mijnb. 55, 179–184.

Schlanger, S.O., Jenkyns, H.C., Premoli Silva, I., 1981. Volcanism and vertical tectonics in the Pacific Basin related to global Cretaceous transgressions. Earth Planet. Sci. Lett. 52, 435–449. https://doi.org/10.1016/0012-821X(81)90196-5.

Schoene, B., Eddy, M.P., Samperton, K.M., Keller, C.B., Keller, G., Adatte, T., Khadri, S.F. R., 2019. U-Pb constraints on pulsed eruption of the Deccan Traps across the end-Cretaceous mass extinction. Science 363, 862–866. https://doi.org/10.1126/science.aau2422.

Schroeder, W.H., Munthe, J., 1998. Atmospheric mercury - an overview. Atmos. Environ. 32, 809–822. https://doi.org/10.1016/S1352-2310(97)00293-8.

Selby, D., 2007. Direct Rhenium-Osmium age of the Oxfordian-Kimmeridgian boundary, Staffin bay, Isle of Skye, UK, and the Late Jurassic time scale. Nor. J. Geol. 87, 291–299.

Selby, D., Creaser, R.A., 2003. Re–Os geochronology of organic rich sediments: an evaluation of organic matter analysis methods. Chem. Geol. 200, 225–240. https://doi.org/10.1016/S0009-2541(03)00199-2.

Self, S., Widdowson, M., Thordarson, T., Jay, A.E., 2006. Volatile fluxes during flood basalt eruptions and potential effects on the global environment: a Deccan perspective. Earth Planet. Sci. Lett. 248, 518–532. https://doi.org/10.1016/j.epsl.2006.05.041.

Selin, N.E., 2009. Global biogeochemical cycling of mercury: a review. Annu. Rev. Environ. Resour. 34, 43–63. https://doi.org/10.1146/annurev.environ.051308.084314.

Shen, J., Algeo, T.J., Chen, J., Planavsky, N.J., Feng, Q., Yu, J., Liu, J., 2019a. Mercury in marine Ordovician/Silurian boundary sections of South China is sulfide-hosted and non-volcanic in origin. Earth Planet. Sci. Lett. 511, 130–140. https://doi.org/10.1016/j.epsl.2019.01.028.

Shen, J., Chen, J., Algeo, T.J., Yuan, S., Feng, Q., Yu, J., Zhou, L., O'Connell, B., Planavsky, N.J., 2019b. Evidence for a prolonged Permian–Triassic extinction interval from global marine mercury records. Nat. Commun. 10 https://doi.org/10.1038/s41467-019-09620-0.

Shen, J., Feng, Q., Algeo, T.J., Liu, J., Zhou, C., Wei, W., Liu, J., Them II, T.R., Gill, B.C., Chen, J., 2020. Sedimentary host phases of mercury (Hg) and implications for use of Hg as a volcanic proxy. Earth Planet. Sci. Lett. 543, 116333. https://doi.org/10.1016/j.epsl.2020.116333.

Sliter, W.V., 1989. Aptian anoxia in the Pacific Basin. Geology 17, 909–912. https://doi.org/10.1130/0091-7613(1989)017<0909:AAITPB>2.3.CO;2.

Storm, M.S., Hesselbo, S.P., Jenkyns, H.C., Ruhl, M., Ullmann, C.V., Xu, W., Leng, M.J., Riding, J.B., Gorbanenko, O., 2020. Orbital pacing and secular evolution of the Early Jurassic carbon cycle. Proc. Natl. Acad. Sci. U. S. A. 117, 3974–3982. https://doi.org/10.1073/pnas.1912094117.

Svensen, H., Planke, S., Malthe-Sørenssen, A., Jamtveit, B., Myklebust, R., Eidem, T.R., Rey, S.S., 2004. Release of methane from a volcanic basin as a mechanism for initial Eocene global warming. Nature 429, 542–545. https://doi.org/10.1038/nature02566.

Svensen, H., Percival, L.M.E., Jones, M.T., Mather, T.A., 2018. Release of mercury from black shale during contact metamorphism and the implications for mercury as a volcanic proxy. In: Geophysical Research Abstracts, 20, EGU2018-10291-1. EGU General Assembly.

Tarduno, J.A., Sliter, W.V., Bralower, T.J., McWilliams, M., Premoli Silva, I., Ogg, J.G., 1989. M-sequence reversals recorded in DSDP sediment cores from the western Mid-Pacific Mountains and Magellan Rise. Geol. Soc. Am. Bull. 101, 1306–1316. https://doi.org/10.1130/0016-7606(1989)101<1306:MSRRID>2.3.CO;2.

Taylor, B., 2006. The single largest oceanic plateau: Ontong Java–Manihiki–Hikurangi. Earth Planet. Sci. Lett. 241, 372–380. https://doi.org/10.1016/j.epsl.2005.11.049.

Tedeschi, L.R., Jenkyns, H.C., Robinson, S.A., Lana, C.C., Menezes Santos, M.R.F., Tognoli, F.M.W., 2020. Aptian carbon-isotope record from the Sergipe-Alagoas Basin: New insights into oceanic anoxic event 1a and the timing of seawater entry into the South Atlantic. Newsl. Stratigr. 53, 333–364. https://doi.org/10.1127/nos/2019/0529.

Tegner, C., Storey, M., Holm, P.M., Thorarinsson, S.B., Zhao, X., Lo, C.H., Knudsen, M.F., 2011. Magmatism and Eurekan deformation in the High Arctic Large Igneous Province: ^{40}Ar-^{39}Ar age of Kap Washington Group volcanics, North Greenland. Earth Planet. Sci. Lett. 303, 203–214. https://doi.org/10.1016/j.epsl.2010.12.047.

Tejada, M.L.G., Suzuki, K., Kuroda, J., Coccioni, R., Mahoney, J.J., Ohkouchi, N., Sakamoto, T., Tatsumi, Y., 2009. Ontong Java Plateau eruption as a trigger for the early Aptian oceanic anoxic event. Geology 37, 855–858. https://doi.org/10.1130/G25763A.1.

Them, T.R., Jagoe, C.H., Caruthers, A.H., Gill, B.C., Grasby, S.E., Gröcke, D.R., Yin, R., Owens, J.D., 2019. Terrestrial sources as the primary delivery mechanism of mercury to the oceans across the Toarcian Oceanic Anoxic Event (Early Jurassic). Earth Planet. Sci. Lett. 507, 62–72. https://doi.org/10.1016/j.epsl.2018.11.029.

Thiede, J., et al., 1981. Site 463: western mid-Pacific mountains. In: Initial Reports of the Deep Sea Drilling Project, 62, pp. 33–156. https://doi.org/10.2973/dsdp.proc.62.102.1981.

Thiede, J., Dean, W.E., Claypool, G.E., 1982. Oxygen-deficient depositional paleoenvironments in the mid-Cretaceous tropical and sub-tropical central Pacific Ocean. In: Schlanger, S.O., Cita, M.B. (Eds.), Nature and origin of Cretaceous Carbon-rich Facies. Academic Press, London, pp. 79–100.

Thordarson, T., 2004. Accretionary-lapilli-bearing pyroclastic rocks at ODP Leg 192 Site 1184: a record of subaerial phreatomagmatic eruptions on the Ontong Java Plateau. In: Fitton, J.G., Mahoney, J.J., Wallace, P.J., Saunders, A.D. (Eds.), Origin and Evolution of the Ontong Java Plateau, Geological Society of London, Special Publications, 229, pp. 275–306. https://doi.org/10.1144/GSL.SP.2004.229.01.16.

Turgeon, S.C., Creaser, R.A., 2008. Cretaceous oceanic anoxic event 2 triggered by a massive magmatic episode. Nature 454, 323–326. https://doi.org/10.1038/nature07076.

Vallier, T.L., Jefferson, W.S., 1981. Volcanogenic sediments from Hess Rise and the mid-Pacific mountains, Deep Sea Drilling Project Leg 62. In: Thiede, J., Vallier, T.L., et al. (Eds.), Initial Reports of the Deep Sea Drilling Project, 62, pp. 545–557. https://doi.org/10.2973/dsdp.proc.62.119.1981.

van Acken, D., Thomson, D., Rainbird, R.H., Creaser, R.A., 2013. Constraining the depositional history of the Neoproterozoic Shaler Supergroup, Amundsen Basin, NW Canada: rhenium-osmium dating of black shales from the Wynniatt and Boot Inlet Formations. Precambrian Res. 236, 124–131. https://doi.org/10.1016/j.precamres.2013.07.012.

van Breugel, Y., Schouten, S., Tsikos, H., Erba, E., Price, G.D., Sinninghe Damsté, J.S., 2007. Synchronous negative carbon isotope shifts in marine and terrestrial biomarkers at the onset of the early Aptian oceanic anoxic event 1a: evidence for the release of ^{13}C-depleted carbon into the atmosphere. Paleoceanography 22. https://doi.org/10.1029/2006PA001341.

Vickers, M.L., Price, G.D., Jerrett, R.M., Watkinson, M., 2016. Stratigraphic and geochemical expression of Barremian–Aptian global climate change in Arctic Svalbard. Geosphere 12, 1594–1605. https://doi.org/10.1130/GES01344.1.

Wang, S., Shao, L.Y., Yan, Z.M., Shi, M.J., Zhang, Y.H., 2019. Characteristics of Early Cretaceous wildfires in peat-forming environment, NE China. J. Palaeogeogr. 8 https://doi.org/10.1186/s42501-019-0035-5.

Weissert, H., 1989. C-isotope stratigraphy, a monitor of paleoenvironmental change: a case study from the Early Cretaceous. Surv. Geophys. 10, 1–61. https://doi.org/10.1007/BF01901664.

Westermann, S., Stein, M., Matera, V., Fiet, N., Fleitmann, D., Adatte, T., Föllmi, K.B., 2013. Rapid changes in the redox conditions of the western Tethys Ocean during the early Aptian oceanic anoxic event. Geochim. Cosmochim. Acta 121, 467–486. https://doi.org/10.1016/j.gca.2013.07.023.